Full Length Article

The ALPHA-2 apparatus - facilitating experimentation with trapped antihydrogen

R. Akbari [a], B.X.R. Alves [b], C.J. Baker [c], M. Baquero-Ruiz [d], W. Bertsche [e,f], E. Butler [g], C. Burrows [c], A. Capra [h], C.L. Cesar [i], M. Charlton [c], R. Collister [h], A. Cridland [c], S. Eriksson [c], A. Evans [j], L.T. Evans [k], N. Evetts [l], J. Fajans [k], T. Friesen [b,j], M.C. Fujiwara [h], D.R. Gill [h], P. Grandemange [h,j], P. Granum [b], A. Gutierrez [l], J.S. Hangst [b], M.E. Hayden [m], D. Hodgkinson [k,f], C.A. Isaac [c], A. Ishida [n], M.A. Johnson [e,f], J.M. Jones [c], S.A. Jones [c,o], S. Jonsell [p], A. Khramov [h], L. Kurchaninov [h], A. Little [k], N. Madsen [c], D. Maxwell [c], J.T.K. McKenna [h], S. Menary [q], J.M. Michan [h,d], T. Momose [a], P.S. Mullan [c,r], K. Olchanski [h], A. Olin [h,s], J. Peszka [r,c], A. Povilus [t], A. Powell [j], P. Pusa [u], C.Ø. Rasmussen [b,g], R.L. Sacramento [i], M. Sameed [c,f], E. Sarid [v,w], D.M. Silveira [i], C. So [h,j], S. Stracka [x], G. Stutter [b], T.D. Tharp [y],*, R.I. Thompson [j], C. Torkzaban [k], D.P. van der Werf [c], J.S. Wurtele [k]

a Department of Chemistry, University of British Columbia, Vancouver BC, V6T 1Z4, Canada
b Department of Physics and Astronomy, Aarhus University, DK 8000, Aarhus C, Denmark
c Department of Physics, Faculty of Science and Engineering, Swansea University, Swansea SA2 8PP, United Kingdom
d Ecole Polytechnique Federale de Lausanne (EPFL), Swiss Plasma Center (SPC), CH-1015, Lausanne, Switzerland
e The Cockcroft Institute, Warrington, WA4 4AD, United Kingdom
f School of Physics and Astronomy, University of Manchester, Manchester, M13 9PL, United Kingdom
g Experimental Physics Department, CERN, CH-1211, Geneva 23, Switzerland
h TRIUMF, 4004 Wesbrook Mall, Vancouver BC, Canada V6T 2A3
i Instituto de Fisica, Universidade Federal do Rio de Janeiro, Rio de, Janeiro 21941-972, Brazil
j Department of Physics and Astronomy, University of Calgary, Calgary AB, T2N 1N4, Canada
k Department of Physics, University of California at Berkeley, Berkeley, California 94720-7300, USA
l Department of Physics and Astronomy, University of British Columbia, Vancouver BC, V6T 1Z4, Canada
m Department of Physics, Simon Fraser University, Burnaby BC, V5A 1S6, Canada
n Department of Physics, The University of Tokyo, 7-3-1 Hongo, Bunkyo, Tokyo 113-0033, Japan
o Van Swinderen Institute for Particle Physics and Gravity, University of Groningen, 9747 AG Groningen, The Netherlands
p Department of Physics, Stockholm University, SE 10691, Stockholm, Sweden
q Department of Physics and Astronomy, York University, Toronto ON, M3J 1P3, Canada
r Institute for Particle Physics and Astrophysics, ETH Zurich, Zurich, Switzerland
s Department of Physics and Astronomy, University of Victoria, Victoria BC, Canada V8P 5C2
t Lawrence Livermore National Laboratory (LLNL), 7000 East Ave., Livermore, CA 94550, United States
u Department of Physics, University of Liverpool, Liverpool L69 7ZE, UK
v Soreq NRC, Yavne, 81800, Israel
w Department of Physics, Ben Gurion University, Beer Sheva, Israel
x Universita di Pisa, and Sezione INFN di Pisa, Largo Pontecorvo 3, 56127 Pisa, Italy
y Department of Physics, Marquette University, P.O. Box 1881, Milwaukee, WI 53201-1881, USA

ARTICLE INFO

ABSTRACT

This paper describes the ALPHA-2 apparatus, used at the CERN Antiproton Decelerator facility for the study of trapped antihydrogen atoms. Details of both the construction and performance are included. Prominence is given to both the new and the improved features, with respect to the original ALPHA assembly, of the apparatus including a stand-alone antiproton catching trap, the traps used to mix antiparticles to produce the

* Corresponding author.
 E-mail address: timothy.tharp@marquette.edu (T.D. Tharp).

Microwaves
Silicon vertex detector

anti-atoms, the magnetic atom trap used to hold some of them, and access for laser light to facilitate excitation of the antihydrogen $1S$-$2P$ and $1S$-$2S$ transitions.

1. Introduction

Antihydrogen ($\overline{\mathrm{H}}$) was first created under controlled conditions in 2002 by the mixing of positrons (e^+) and antiprotons ($\overline{p}$) in Penning-trap like apparatus [1,2]. This advance was followed by several studies of aspects of the dynamics of $\overline{\mathrm{H}}$ formation, leading to the conclusion that the anti-atom was formed predominantly via a three-body reaction ($\overline{p} + e^+ + e^+ \rightarrow \overline{\mathrm{H}} + e^+$) involving antiproton interactions in dense ($\sim 10^{14}$ m^{-3}), cold (< 100 K) positron plasmas [3–10]. Some of these studies (in particular [7,10]) concluded that the simple e^+-$\overline{p}$ mixing procedures used in these early experiments were unlikely to result in significant yields of antihydrogen suitable for capture in magnetic minimum atom traps, which typically have a maximum well depth of around 0.5 K. The apparatus used by the ATHENA collaboration for their work during this period has been described in detail elsewhere [11].

The next generation of antihydrogen apparatus, designed expressly to achieve anti-atom trapping, was developed by the ALPHA collaboration [12]; this apparatus achieved trapping, accumulation and eventually confinement lifetimes in excess of 60 h [13–17]. Antihydrogen trapping has also been demonstrated by the ATRAP experiment [18]. The ALPHA apparatus was further used to: (i) detect the first quantum jump in an anti-atomic system [19] (involving a microwave-induced ground-state hyperfine transition); (ii) to set crude bounds on the gravitational behaviour of antihydrogen [20]; and (iii) to probe a putative electrical charge on the anti-atom [21,22], leading (indirectly) to an improved comparison of the positron and electron charges.

The apparatus used for ALPHA's pre-2017 investigations [12], though considerably evolved from the ATHENA hardware [11], nevertheless contained the antiproton capture and cooling sections alongside the antihydrogen formation and trapping regions. Such a compact design was found to be unsuited to furthering the experimental investigation of antihydrogen, most evidently because it did not have any laser access pathways which would be required for the long-anticipated spectroscopic studies of the trapped anti-atom [23,24]. Thus, we present here a full description of a new experimental system, the ALPHA-2 apparatus. This device incorporates (amongst other novel features): (i) facilities for laser access for 121.6 nm (the vacuum ultraviolet wavelength of the hydrogen/antihydrogen $1S$-$2P$ transition) and 243.0 nm (the wavelength required for the 2-photon $1S$-$2S$ spectroscopy transition) and an internal cavity to build up power for the 243 nm light (see e.g. [25] for a measurement of the corresponding line in hydrogen); (ii) a new $\overline{p}$ Catching Trap for manipulation and storage of antiprotons, with an accompanying transfer line to move the antiparticles to the $\overline{\mathrm{H}}$ formation and trapping region; (iii) a new cryogenic system with an improved (lower) base temperature and a reduced consumption of liquid helium; (iv) a multi-coil (superconducting) design for the magnetic minimum Atom Trap for the manipulation of trapped $\overline{\mathrm{H}}$ which provides the advantage of being able to produce a flatter field region to increase the interaction rate between the atoms and the laser(s); (v) upgraded silicon vertex detector capabilities and renovations to the positron accumulation and transfer systems, and (vi) an improved system for microwave ingress.

This apparatus has been successfully deployed to characterise the antihydrogen ground state splitting [26], to observe and characterise the two-photon $1S$-$2S$ transition [27,28], to stack antihydrogen and observe the $1S$-$2P$ Lyman-α line [17], and most recently to achieve laser cooling of the anti-atom [29] and perform a spectroscopic investigation on the cooled sample [30].

In addition to the capabilities reported herein, additional upgrades are underway. New developments not reported here include (i) the incorporation of CERN's new ELENA ring for improved antiproton deceleration, and (ii) the ALPHA-g apparatus for gravitational studies [31–33].

The apparatus we describe is located at the so-called Antimatter Factory at CERN, which is comprised of the Antiproton Decelerator and the low energy antiproton ring, ELENA. There is a thriving experimental community based there which, in addition to ALPHA, is currently made up of the AEgIS, ASACUSA, BASE, GBAR and PUMA collaborations. AEgIS and GBAR plan to study the gravitational interaction of antihydrogen and both have recently reported the production of antihydrogen via the interactions of antiprotons with positronium (an electron–positron pair) [34,35]. ASACUSA has produced an antihydrogen beam using positron–antiproton mixing [36] which it intends to use for comparative studies of the hydrogen-antihydrogen ground state hyperfine splitting (see, e.g., [37]). This collaboration has also pioneered the study of antiprotonic helium for tests of few-body and fundamental physics: see [38] for a recent example. BASE tests fundamental symmetries by making precision comparisons of antiproton and proton properties such as the charge-to-mass ratio [39] and magnetic moment [40,41]. PUMA is the most recent addition to the Antimatter Factory and plans to develop a portable trap system to transport antiprotons to ISOLDE, CERN's isotope facility, to study their interaction and annihilation with nuclei [42].

The bulk of our presentation of the ALPHA-2 apparatus and its capabilities is contained in Section 3, which is divided into several subsections covering the components of the apparatus and their performance. Concluding remarks are given in Section 4, whilst Section 2 contains an overview of ALPHA-2, including a more detailed exposition of the rationale for its development.

2. Apparatus overview

A schematic illustration of ALPHA-2 is presented in Fig. 1. The **Antiproton Decelerator** delivers antiprotons to the **Antiproton Catching Trap**, which captures and manipulates (on the order of 10^5) antiprotons. The **Positron Accumulator** prepares (on the order of 10^7) positrons. When both antiparticle populations are prepared they are delivered to the **Mixing and Atom Trap**, which performs two essential functions: (i) manipulation and controlled mixing of the two populations to promote antihydrogen formation, and (ii) trapping a subset of the resulting anti-atoms using the interaction between their magnetic moment and a carefully tailored magnetic field geometry. The Mixing and Atom Trap includes several sub-systems. The **Mixing Trap** is a specialised Penning-Malmberg trap used to manipulate the antiparticle plasmas and gently mix them to form cold antihydrogen. The superconducting **Atom Trap** uses an octupole magnet and magnetic mirror coils to produce a minimum in the magnetic field magnitude ($|\vec{B}|$), which is used to trap the neutral antihydrogen atoms. These sub-systems are immersed in liquid helium (at 4.2 kelvin) using a **Cryogenic System** which enables the low temperature conditions required for cold plasmas as well as the operation of superconducting magnets. **Diagnostic Manipulators** house a variety of instruments which are used to optimise non-neutral plasmas for mixing. Once antihydrogen atoms are formed and trapped, they are interrogated using **Laser Systems** and a **Microwave Injection System**, while annihilation position data are collected using a **Silicon Vertex Detector**.

ALPHA's physics programme, in common with all current low energy antiproton work, takes place at the **Antiproton Decelerator** (AD) which is a unique facility [43–45] located at CERN, the European Particle Physics Laboratory. The AD provides pulses of around 3×10^7 antiprotons every 100 s or so, each with a duration of 200 ns and at a kinetic energy of 5.3 MeV. The use of machine triggers, energy degradation and fast high voltage switching on trap electrodes (see Section 3.1) allows about 0.1% of the incoming pulse to be captured
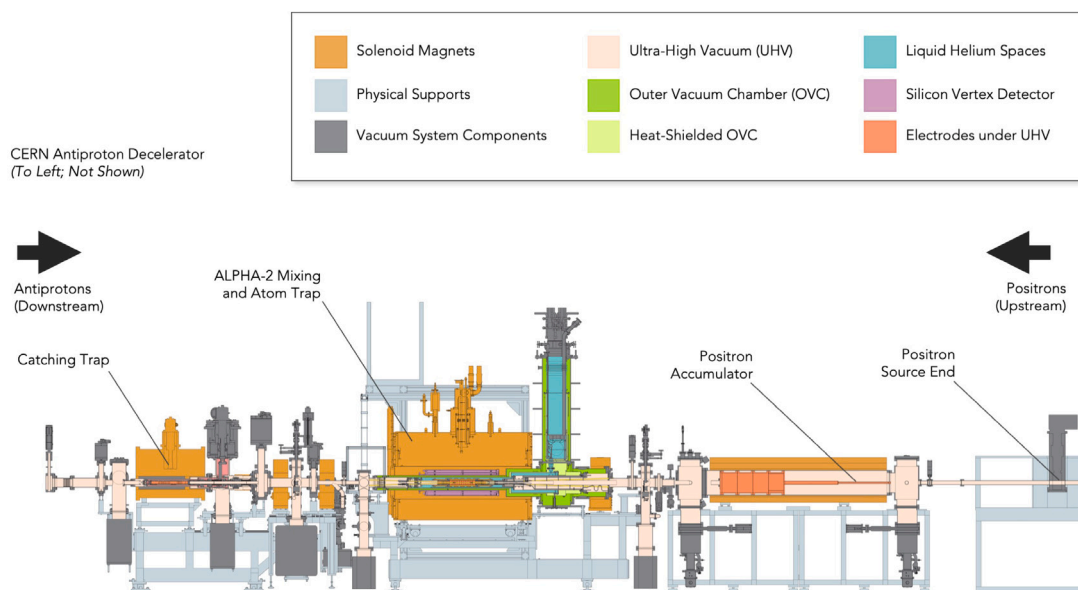
Fig. 1. An overview schematic of the ALPHA-2 apparatus in its 2017–19 configuration. The major sections of the ALPHA-2 apparatus include the Catching Trap (left), the Mixing and Atom Trap (centre), and the Positron Accumulator (right).

for further experimentation. The sequence of antiproton manipulations required to form and trap antihydrogen, which can involve cloud compression [46] and evaporative cooling of both the positrons and antiprotons [47], plus the duration of any experiment on the trapped anti-atoms (see e.g., [27,28]), routinely exceeds the 100 s separation between the AD pulses, thus not all AD pulses can be used.

The desire to use more of the available antiprotons has, in part, motivated the incorporation of the stand alone **Antiproton Catching Trap** (Section 3.1) into ALPHA-2. This device makes the accumulation and manipulation of antiprotons essentially independent of the remainder of the experiment: effectively ALPHA-2 contains its own antiproton reservoir, which it can empty and fill as desired, in essence de-coupling antihydrogen experimentation from the AD machine cycles. This allows for dramatic enhancements in the efficiency of antiproton utilisation, as well as much more efficient experiment operation.

CERN has recently added the ELENA ring to its antiproton facilities [45,48]. This provides additional improvements beyond those reported here since ELENA further decelerates the antiparticles to 100 keV, resulting in around a factor of up to 100 increase in the captured yield. Furthermore, the lower beam kinetic energy has resulted in the use of electrostatic elements for beam transport and delivery, to facilitate rapid experiment-to-experiment transfer of the antiproton pulses.

The **Positron Accumulator** (Section 3.2) is a stand-alone instrument which has its origins in the apparatus developed for the ATHENA experiment [49]. The device is a Na-22 based 3-stage buffer gas accumulator of the type developed by Surko and co-workers (see e.g., [50]). This type of accumulator, which was first suggested for application to antihydrogen experimentation in the late nineties [51], has the advantage of being able to capture positrons over time periods commensurate with the AD cycle time and is typically routine and reliable in performance. Such devices have now been adopted by all antihydrogen collaborations (see e.g., [52–54]); the ATRAP and GBAR collaborations have each reported more than 10^9 positrons stored in a cryogenic trap [55,56].

Antihydrogen is formed in the **Mixing and Atom Trap**, shown in the central region of Fig. 1. While the Mixing Trap and the Atom Trap necessarily coexist in the same physical space, they are distinct systems which perform distinct functions. The **Mixing Trap** (Section 3.3) uses electrodes, arranged in Penning-Malmberg trap configurations, to prepare antiprotons and positrons independently, then

mix the two populations under controlled conditions. To tailor the electron, positron, and antiproton charged particle clouds, or plasmas, rotating wall compression [46,57–60] and evaporative cooling [47,61] are employed.

In the same physical location, the **Atom Trap** (Section 3.5) forms a magnetic field which is capable of trapping a subset of the neutral antihydrogen atoms that are formed. Confinement of the antihydrogen atoms is accomplished by using the interaction between their magnetic moment and a carefully tailored magnetic field geometry. The octupole field coil provides a magnetic field with a large radial gradient, resulting in radial confinement of antihydrogen atoms with kinetic energies below the well depth, which is around 0.5 K equivalent. Axial confinement is achieved using the mirror coils. The rationale for choosing such an arrangement has been described elsewhere [12,62]. Whereas the original ALPHA apparatus [12] only contained a pair of mirror coils to longitudinally confine the anti-atoms, ALPHA-2 has 5 such coils which can be used, for instance, to tailor the magnetic field to aid spectroscopic investigation of the trapped antihydrogen atoms.

The **Cryogenic System** (Section 3.6) is necessary to achieve the low plasma temperatures needed for antihydrogen production, and is also used to cool the superconducting magnets.

Transfer Magnets (Section 3.7) are used to facilitate the transfer of antiprotons (from the Catching Trap) and positrons (from the Positron Accumulator) into the Mixing and Atom Trap.

Laser Systems (Section 3.8) are used to excite the low-lying transitions in antihydrogen for spectroscopy of the anti-atom, and to perform laser cooling on a trapped sample. Separate laser installations have been developed to provide light at wavelengths of 243.0 nm (for the two-photon, Doppler-free, $1S$-$2S$ transition) and 121.6 nm (for the $1S$-$2P$ transition). These devices, the specialised optics used to deliver the light to the antihydrogen trapping region, and the 243 nm light power build-up cavity, situated in the cryogenic region of the trap, are described in more detail in Section 3.8.

The **Microwave Injection System** (Section 3.9) is used to excite antihydrogen hyperfine transitions.

The **Silicon Vertex Detector** (Section 3.10) is used to identify the charged products, mostly charged pions, of the antiproton annihilation. The annihilation location, or vertex, is determined by reconstructing the trajectories of those particles from their interactions with the silicon modules.
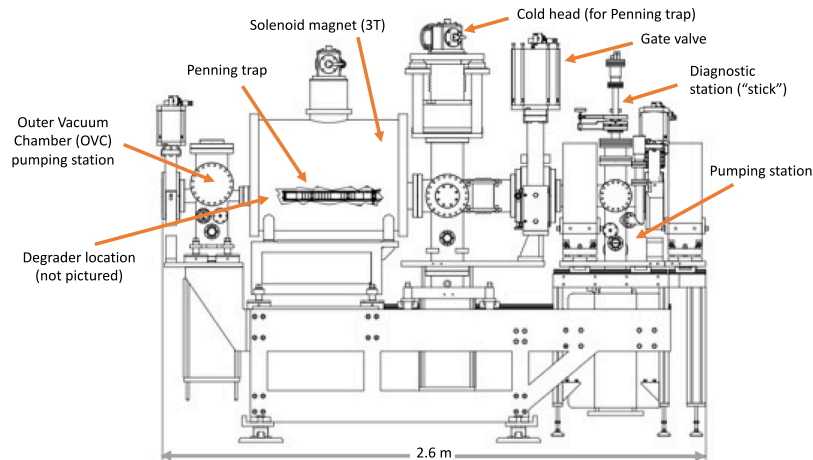
Fig. 2. Schematic of the Catching Trap and Transfer Magnet section of the ALPHA-2 apparatus. A cutaway shows the Penning-Malmberg trap inside the cryo-cooled magnet chamber. Not shown to the left of this diagram lies the evacuated beamline of the AD. Not shown to the right, an evacuated beamline connects to the Mixing and Atom Traps.

3. Apparatus - description and performance

3.1. The antiproton catching trap

3.1.1. Catching trap overview

The Catching Trap, shown in Fig. 2, is used to capture, accumulate, and manipulate antiprotons ejected from the AD for use in the main ALPHA-2 apparatus (see Fig. 1), and is described in detail in this section. The trap typically captures around 10^5 antiprotons per AD cycle [16], which are then cooled (by sympathetic cooling with electrons) and stored until the Mixing Trap is ready to accept them.

3.1.2. Vacuum system and performance

Vacuum requirements for the long-term storage of antiprotons are strict. Whilst neutral and ionised residual gas can drive radial transport in confined plasmas leading to particle loss, annihilation with the background gas is a larger concern for confined antimatter plasmas. Thus, vacuum design for the Catching Trap is motivated to achieve a pressure low enough to confine antiprotons for over a day without significant loss.

The annihilation rate of antiprotons with hydrogen atoms (which we use as a proxy for molecular hydrogen, which is likely to be the main impurity under cryogenic conditions) has been used to estimate the pressure necessary to achieve such storage. Following the treatment in [63], the annihilation cross section, $\sigma_a(H)$ can be estimated to be

$$\sigma_a(H) = 3.6 \times 10^5 \pi r_0^2 (c/v_{\text{rel}}),\qquad(1)$$

where c is the speed of light, v_{rel} is the relative velocity between the antiproton and the atom, and r_0 is the classical electron radius (2.82×10^{-15}) m. This expression is valid when the energies of the particles are in the kinetic energy range between 10^{-5} and 0.1 eV (with a corresponding temperature range of 0.1-10^3 K). The cross section can in turn be used to estimate a pressure, P, given an annihilation lifetime, τ, via the relation

$$P = \frac{k_B T}{\tau \sigma_a(H) v_{\text{rel}}},\qquad(2)$$

where T is the gas temperature and k_B is Boltzmann's constant.

In our case, the temperature of the typical stored plasma (before cooling) is likely to be about 0.1 eV, and as such is significantly higher than the anticipated temperature of the background gas within our 4 K (0.3 meV) cryostat, and consequently the main contributor to v_{rel}. For an antiproton lifetime of 10^6 s, or roughly 12 days, the pressure would need to be in the 10^{-13}–10^{-14} mbar range. This level of vacuum is not achievable through conventional pumping methods, however cryopumping by cold surfaces in the trap space makes this feasible.

Residual gas vapour pressures are strongly dependent upon temperature, such that cryopumping surfaces should be as cold as possible to achieve the lowest pressures. Even with a surface temperature of 4 K, helium and hydrogen gases have significant saturation vapour pressures of $\sim 10^{-2}$ mbar and $\sim 10^{-6}$ mbar respectively [64,65], though only after a full monolayer of the gas in question is frozen onto the trap surfaces. This is easily avoided by keeping the gas load on the cryogenics space low [63].

In the present configuration of the Catching Trap, the room temperature section of the device is sealed with all-metal valves and pumped with a 400 Ls^{-1} triode ion pump. Pressures achieved in the room temperature section after baking are typically around 5×10^{-10} mbar. Performance of the vacuum is monitored via annihilations [66]. Antiproton lifetimes in the Catching Trap typically vary from tens of minutes to tens of hours depending on vacuum conditions. (We note that this is not a record for lowest vacuum pressure experimentally achieved: the BASE collaboration [67] have reported development of a reservoir with an antiproton lifetime of around 1 yr, implying a base pressure in the 10^{-15} mbar region or below.)

3.1.3. Cryogenics system

The primary purpose of the cryogenics system in the Catching Trap is to enable and create low vacuum in the antiproton (Penning-Malmberg) trap to maximise the annihilation lifetime, τ. Cooling is accomplished through the use of a Sumitomo RDK-408D2 Gifford-MacMahon cryogenic refrigerator. The device has two physical stages of heat exchange that achieve different equilibrium temperatures under different heat loads, with the second stage ideally reaching 4 K. Fig. 3 shows a map of the temperatures of the two stages for differing heat loads.

The two primary heat loads on the Catching Trap are from thermal radiation on the trap and vacuum surfaces, and static heat conduction from room temperature to colder parts, with the former dominating and originating from room temperature black body radiation. This load is mitigated by a radiation shield, shown in Fig. 4, in the form of a cylindrical copper cap which surrounds the trap, its vacuum chamber and the thermal links from the nominally 4 K structures to room temperature. This so-called "40 K shield" is connected to the first stage of the cryocooler and is thermally isolated from room temperature inside a cryostat vacuum that is independent of the trap vacuum system. The pressure in this system is better than 1×10^{-6} mbar before cooling.

The shield is supported with G-10 (fibreglass laminate) mechanical structures designed to minimise static thermal conductivity from room temperature to the shield and from the shield to nominally 4 K areas of the apparatus. The shield was polished and plated with gold to
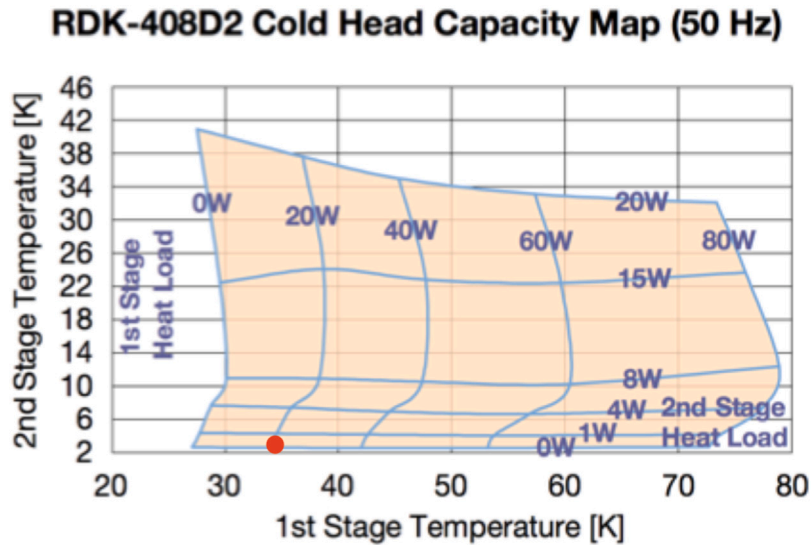
RDK-408D2 Cold Head Capacity Map (50 Hz)

Fig. 3. Cryocooler map for the RDK-408D2 system provided by Sumitomo Heavy Industries (SHI) Cryogenics Group (https://shicryogenics.com), reprinted with permission. The estimated operating point for the ALPHA Catching Trap is ~20 W on the first stage and ~200 mW on the second stage, as denoted by the red dot.
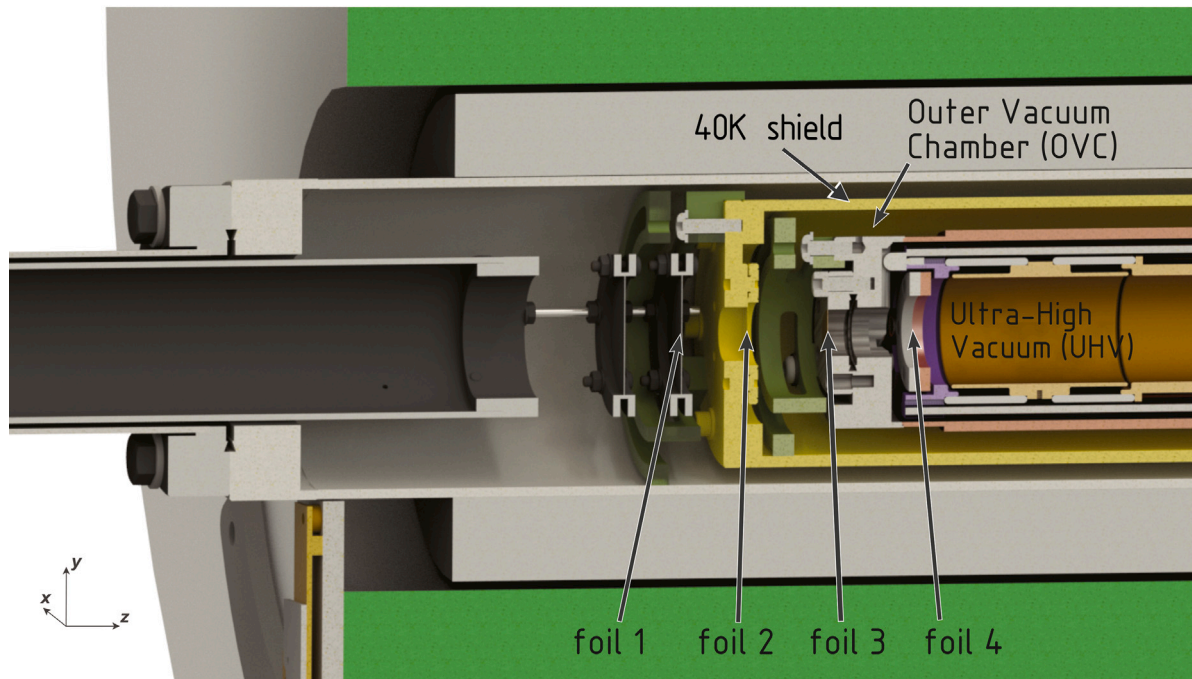

Fig. 4. Schematic of the cryogenic space of the Catching Trap. The 40 K shield helps to prevent thermal radiation from reaching the electrodes. Antiprotons enter the Catching Trap by passing through the degrader foils; while some annihilations occur, a large number of those that do not annihilate lose enough energy to become trappable by the 5 kV high voltage electrodes. (Note that with the advent of ELENA, the degrader shown here was replaced by a single thin foil.)

increase reflectivity, and the structure is also clamped to a special copper flange which provides a high thermal conductivity path into the trap vacuum space for the purposes of heat sinking warm-end trap structures and cabling. Considering both radiation and expected static conduction loads, the heat load on the 40 K shield, and hence the first stage of the cryocooler, is estimated to be ∼ 20 W. The geometry of the 40 K Shield is shown in Fig. 4.

The trap is contained within an independent vacuum (the space labelled "UHV" in Fig. 4). The vacuum vessel directly surrounding the trap is manufactured from gold-plated OFHC copper with stainless steel flanges brazed onto either end. This vessel is heat sunk through an interconnection system of copper bars and flexible copper braid to the second stage of the cryocooler. As this vacuum chamber directly

connects out to room temperature, the cold portion of this vessel is thermally isolated through the use of thermal breaks on the axis of the trap consisting of stainless steel edge-welded bellows fixed in place with G-10 spacers. There are bellows between the 4 K vessel and the 40 K heatsink flange mentioned above, as well as between this heatsink and the room temperature structures. We estimate the total heat load from static conduction and thermal radiation on the 4 K structures to be ∼200 mW.

These approximate heat loads (20 W on the first stage and 200 mW on the second stage) result in an operating point on Fig. 3 that is well-covered by the capabilities of the RDK-408D2, and would predict an equilibrium temperature of the second stage of the cryocooler of ∼3.8 K. Operating in this range and keeping these heat loads as low
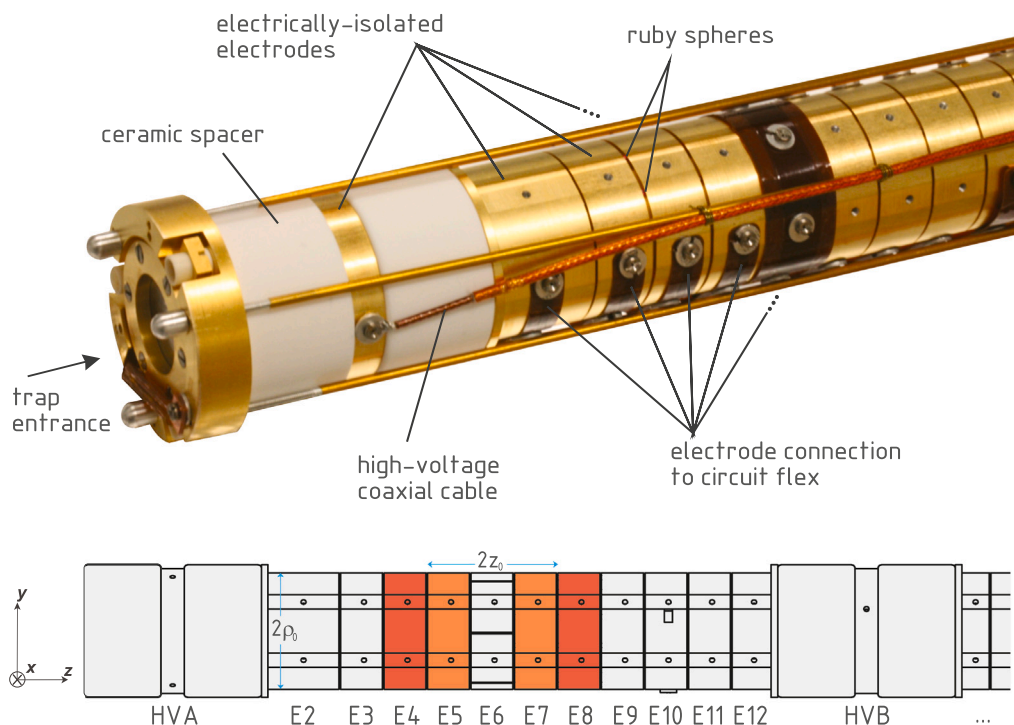
Fig. 5. A photograph (top) and schematic (bottom) of the Catching Trap electrodes. High voltage electrodes (HVA and HVB) are used for the initial antiproton capture; the remaining electrodes are used to manipulate antiproton and electron plasmas.

as practical ensures that the heat conducted to the cryocooler does not create unwanted thermal gradients across the machine.

The Penning trap, shown in Fig. 5, consists of electrically, and hence thermally, isolated electrodes, so heat sinking these structures is challenging, especially since they are connected by cabling directly to room temperature objects. Dealing with the heat load of the cables and heat sinking the traps is accomplished by fabricating the interconnects in flexible circuits which minimise copper cross-section for each signal. The flexible circuits are also designed to be clamped against the outer wall of the chamber to provide a thermal boundary at 4 K and again at 40 K. The circuits are designed in a serpentine fashion to maximise the path length between heat boundaries, while not overly filling the vacuum space with cabling.

Performance of the cryostat is monitored using Lakeshore Cernox CX-SD sensors and Lakeshore temperature controllers. Sensors were glued or clamped to various surfaces including positions on the 40 K shield, the 4 K vessel, trap electrodes, and directly on the first and second stages of the cryocooler. The Cernox resistance is monitored using a 4-point measurement with long leads to ensure thermal isolation of the sensor. Measurements show that the 40 K shield and the 4 K vessel reach temperatures of 39 K and 5 K, respectively, at the relevant point furthest from the cold head. The Penning trap electrodes and structure appear to have temperatures in the range of 4–7 K, with the spread presumably due to differences in the heat-sinking of their specific cable connections. Equilibrium temperatures are reached after cooling from room temperature in approximately 13 h.

3.1.4. Magnet system

The primary axial magnetic field for the Catching Trap is produced by a cryogen-free superconducting solenoid magnet manufactured by Cryogenic Limited. The magnet produces an axially-oriented field with a uniformity better than 1% over a length of 30 cm within a room temperature 14 cm-diameter bore. While the magnet can be operated to 5 T, the nominal operating point for the magnet is 3 T. While a stronger field is generally better for catching and cooling antiprotons, a field that

is too high can be problematic when particles are transferred to lower field regions in subsequent experimental steps due to a radial expansion of the plasma. Fig. 6 shows the nominal axial field, B_z, of the magnet, which has been calculated from a model provided by the company, and verified by direct field measurements performed with a scanning Hall probe instrument.

The field measured for the magnet agrees well with the model in the uniform region of the magnet, but unsurprisingly deviates at the edges of the magnet where manufacturing defects are expected to dominate. The magnetic axis, the cryostat axis, and the Penning trap axis are all independent of one another. In order to ensure alignment of the Penning trap axis with the magnetic axis, direct measurements of the position of an electron plasma extracted onto a micro-channel plate (MCP, see Section 3.1.6) were made from various longitudinal starting positions along the trap axis. The mechanical position of the magnet and its cryostat were adjusted until all plasmas imaged to the same location, indicating that they shared a common field line at the centre of the cryostat. Using this method, and up to the absolute alignment of the Penning trap mechanics, it was possible to align the trap and magnetic axis to within 0.5 mrad. A cross-check between the linear movements required to align the axis along with simulations of this manipulation verify the assumed geometry involved.

Antiprotons are extracted to the Mixing and Atom Trap using magnetic field guiding, as discussed further in Section 3.7. Fringe fields at the end of the magnet tend to result in off-axis offsets to the extracted beam. In order to ensure that antiprotons extract along the centre of the beam line to the Atom Trap, magnetically soft shim material was fixed on the downstream face of the Catching Trap cryostat, and positioned until optimal extraction was achieved. Simulations and measurements show that the amount of material required to achieve this beam has no significant impact on the field lines at the centre of the Penning trap.

3.1.5. Control system

The control system used by the ALPHA Catching Trap is similar in nature to the control system reported in [12]. Fig. 7 shows a block
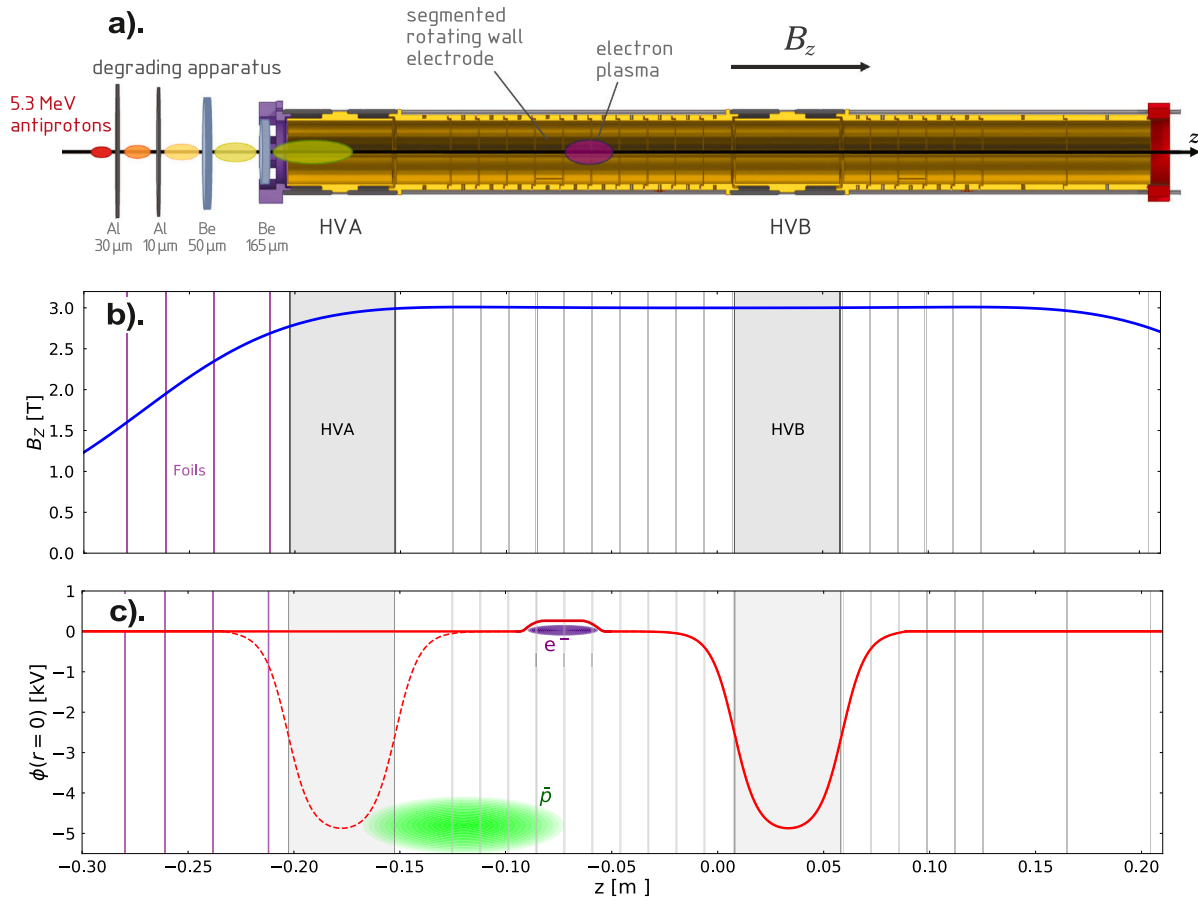
Fig. 6. (a) Rendering of the Catching Trap degraders and Penning trap. (b) Plot of the calculated axial magnetic field, B_z as a function of position. (c) The electric potential at the centre of the trap (at $r = 0$) before (solid line) and after (dotted line) antiproton capture, with representative charged particle clouds. This potential results from the application of discrete voltages to the electrodes.
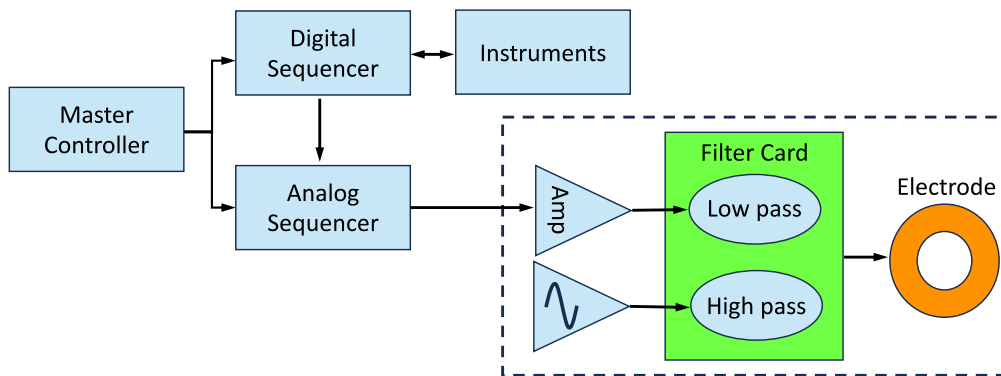

Fig. 7. Block diagram for the Catching Trap timing control. The master controller coordinates timing between digital and analog sequencers. The analog sequencer is primarily responsible for controlling the voltage on trap electrodes. The digital sequencer controls the timing of instruments such as diagnostics.

diagram of the basic elements of the system, as well as electrode connectivity. Central timing for the Catching Trap is controlled by a Master Control programme that sends instructions to digital and analog sequencers. The digital sequencer generates arbitrary digital pulses with a timing resolution of 12.5 ns and jitter of less than 500 ps for deterministic sequences that do not wait for trigger inputs. It is also able to process and respond to input trigger conditions with a jitter of less than 100 ns.

The Catching Trap sequencer has 84 digital output channels capable of driving 5 V TTL lines, and 36 TTL-compatible digital input

lines. The central timing is controlled by a custom control programme developed in LabVIEW™ and operates through a National Instruments PXI-7811R FPGA card. All outputs from the card are connected to a break-out board which buffers the inputs and outputs from the FPGA and achieves TTL electrical compatibility, as well as providing connectors and monitors for the state of the sequencer.

The analog levels used to set the voltages on the electrodes, as well as those on several other devices in the experiment, are established using National Instruments PXI-6733 digital to analog converters (DAC). The master control programme pre-loads a sequence of output voltages
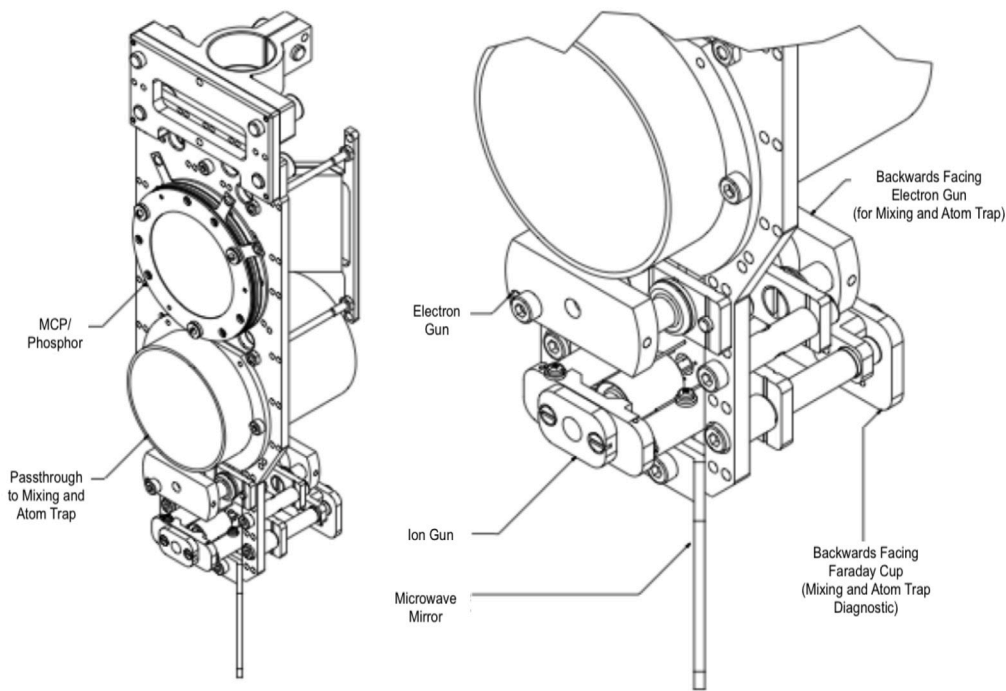
Fig. 8. Features of the Catching Trap diagnostic manipulator. The diagram on the left shows the full instrument panel. In the centre the MCP/Phosphor screen assembly and the grounded pass-through electrode are prominent. The right hand diagram features the electrode and the devices below it in more detail, including the forward- and backward-facing electron guns, the lithium ion source, an Atom Trap Faraday Cup diagnostic and a microwave mirror.

which are updated synchronously via a clock generated by a digital sequencer. The DAC can output voltages in the range from -10 to $+10$ V, with a resolution of 16 bits. In the case of the electrode voltages, the outputs from the DACs are used to drive high voltage amplifiers. These amplifiers nominally have an output range of ±140 V and output bandwidth of 1 MHz. The outputs of these amplifiers are fed through the filter cards which merge low and high frequency signals on an individual electrode.

The filter cards have individual channels for each electrode that combine an input from a low pass filter and a high pass filter. The low pass filter is used to apply the steady voltages on the electrodes, and has an upper cut-off frequency of ∼170 kHz. The high pass filter is used to pass high frequency drives, such as for e-kicks (fast pulses to eject electrons [46]) or rotating wall drives (see Section 3.1.7) to the electrode, and has a lower cut-off frequency of ∼25 kHz.

3.1.6. Diagnostic manipulator

The downstream end of the Catching Trap houses a versatile diagnostic manipulator or "stick." Shown in Fig. 8, this device is a vertically actuated mount in the trap UHV system which contains a number of particle sources and diagnostic instrumentation used to aid in the use of both the Catching Trap and the Mixing and Atom Trap.

Internal to the UHV chamber, elements are mounted to a shaft, encased in bellows and supported by external supports, which is linearly driven using a lag screw. The chamber has a travel range of 15 cm. The stick is driven using a computer-controlled stepper motor, operating at a speed which can travel its full range of motion in approximately 20 s. Absolute tilt and positioning of the stick is achieved through a bellow-decoupled gimbal mechanism, and optical limit stops on either end of the travel. When normally operating, the stick's position is tracked by the stepper motor's internal optical encoder. The absolute position of the device is monitored and logged by the use of a laser ranger oriented in such a way as to measure its extension position.

The primary particle sources used by the Catching Trap are the forward- and backward-facing electron guns. Electrons are important in the ALPHA experiments as tools for sympathetic cooling of the

antiprotons. The Catching Trap utilises Kimball Physics ES-064 Barium Oxide cathodes as electron sources. The barium oxide surface has a relatively low electron work function, which allows operation of the cathode at a temperature of ∼1150 K achieved with a heating current of ∼2.1 A through the cathode surface. Electrons are extracted by biasing the heater power supply to ~-20 V, and thereby accelerated in an electric field of approximately 2500 Vm^{-1} to an energy of ∼10 eV. An extraction current of typically a few 10's of nA is measured on an upstream Faraday Cup, which is sufficient to load the 2×10^{7} electrons typically used to cool antiprotons in a few seconds. There are two such sources installed on the stick, with the primary one facing forwards (towards the Catching Trap) for loading electron plasmas into that trap, and the second facing backwards (away from the Catching Trap) in order to commission the downstream beamline and provide electrons for the Atom Trap.

The stick also has a lithium ion source installed for development work involving heavier ions. ^{6}Li^{+} ions are produced from a source furnished by Heat Wave Labs Inc. and released by heating Li$_2$O-Al$_2$O$_3$-2SiO$_2$ (β-eucryptite salt) embedded in a porous tungsten disc. Using a similar extraction system as the electron cathodes, a ∼1 nA current of ions can be extracted from the source.

In addition to particle sources, the stick also carries a position-sensitive charge detector in the form of a 40 mm-diameter phosphor-backed MCP. The MCP/phosphor assembly is a model APD EDR manufactured by Photonis USA, Inc. This assembly is mounted with the surface of the phosphor screen imaged by a PCO Ag SensiCam CCD camera off axis through a mirror mounted at 45°. Bias voltages for the MCP front, back and phosphor screen are fed through on KAP-5 high voltage cabling. The front surface of the MCP is biased in the range of ±140 V, the rear up to 1200 V and the phosphor screen to 5000 V. The wide range of voltages allows the MCP diagnostic to be used for applications spanning from single-particle-based images of antiprotons and positive ions to line-integrated images of extracted plasmas with 100's of millions of charges. Particles of either sign of charge can be extracted destructively onto the MCP, and the subsequent current created by the amplification channels can illuminate the phosphor screen to
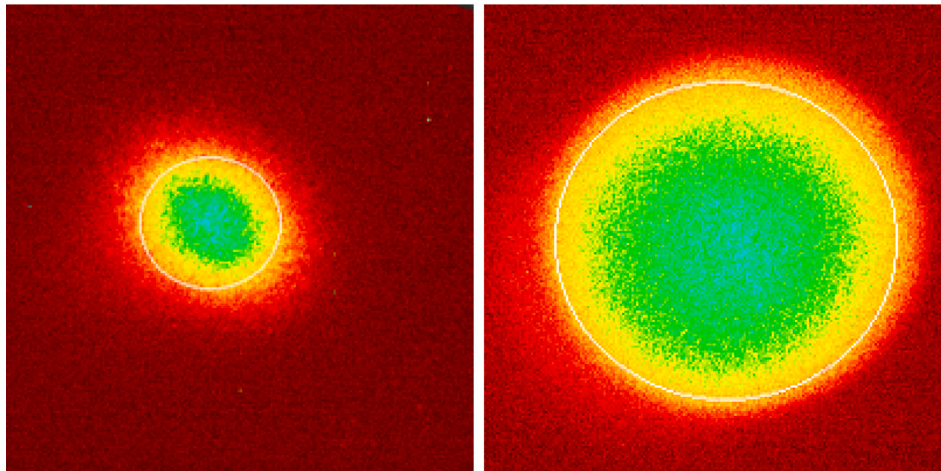
Fig. 9. (Left) MCP/phosphor image of 2.75×10^4 antiprotons with a radius of approximately 2 mm. (Right) MCP/phosphor image of 5.6×10^6 electrons with a radius of approximately 3.7 mm [69]. These plasma images were taken after the application of a rotating wall. The magnification factor due to the reduction of the magnetic field between the Catching Trap and the MCP is 8.3 (see Eq. (5) in Section 3.7), resulting in calculated radii of around 0.25 mm (antiprotons) and 0.45 mm (electrons) in the trap. White circles indicate the approximate plasma size and location as determined by a fit function.

provide spatial information about the plasma. The amplified electronic signal can also be counted to measure the time-resolved current of the extracted particles. Fig. 9 shows a sample images obtained by dumping antiproton and electron plasmas onto the MCP after application of the rotating wall. Operation of this detection system is described in detail in [68].

The stick also holds a backwards-facing (towards the Mixing and Atom Trap) Faraday Cup used for measuring currents extracted upstream from the Mixing and Atom Trap. There is also a grounded pass-through electrode used when transferring particles between the Catching and Mixing Traps.

3.1.7. Penning trap

The heart of the Catching Trap is a Penning-Malmberg trap. This device confines charged particles using a uniform magnetic field B_z (3 T) to provide radial confinement, and electric fields produced by voltages applied to the series of hollow cylindrical electrodes (see Figs. 5 and 6). The Penning Trap electrodes are made of gold-plated aluminum. To maintain a low magnetic susceptibility, we did not plate these using a nickel strike. Instead, the aluminum was electroplated with a layer of copper then a layer of gold.

There are a total of 20 electrodes of varying lengths, producing an overall trap length of ~42 cm. The inner diameter of the electrodes is 29.5 mm with the typical electrode having a length of ~20 mm. Most of the electrodes are simple cylinders with the exception of the "rotating-wall" (RW) electrodes (E6 and E16) that are divided into six equal azimuthal segments with independent electrical control. These sectors can be used to apply non-axisymmetric electric fields to the plasmas to perform the rotating wall manipulations [61].

The majority of the electrodes and their cabling are designed to withstand applied voltages of ± 250 V. The high voltage electrodes (HVA and HVB) and cabling are designed to hold applied voltages of up to 5 kV, which is used to dynamically capture a fraction of the antiprotons emanating from the AD. Electrodes have capacitances on the order of ~50 pF to ground. Cabling to the electrodes contains the majority of a particular electrode circuit's capacitance with values on the order of ~2 nF. Electrode cabling is achieved with the use of transmission lines on custom flexible circuits. These are fed through the inner trap vacuum and out through micro-D feedthroughs into the cryostat outer vacuum chamber. The high voltage cables consist of commercial KAP-5, kapton-insulated coaxial cables which are fed out to air via MHV feedthroughs at room temperature. Cables are clamped against the inner trap wall at nominal temperatures of 4 K and 50 K in order to effectively heat sink

the trap.

In addition to the trap electrodes, the Catching Trap Penning trap structure incorporates a Faraday Cup on the upstream side of the trap which also serves as the final antiproton energy degrading foil. The collection surface of the Faraday Cup/degrader is manufactured from 50 μm beryllium foil. This device, along with its amplifier and readout electronics, can be used for directly counting charge particles ejected onto it. Further, it serves as a radially-centred target onto which cooled antiprotons can be made to annihilate in order to monitor their number. Cernox sensors are also incorporated directly on the trap structure and its electrodes to monitor the temperature of these components. During operation, all measured trap structures equilibrate to temperatures below ~5 K, with the micro-D feedthrough equilibrating to ~50 K.

3.1.8. Annihilation detectors

Two sets of scintillator paddles are used for detecting antiproton annihilations and are located on opposite sides of the trap. Calibration depends on the precise location of the paddles, which are mobile to allow for beamline access; thus, they are most frequently used as an uncalibrated relative diagnostic to tune experimental parameters in order to minimise antiproton losses. Simulations of the scintillators in a fixed position show that detection efficiencies of this system are expected to be 40%–60%.

Each paddle set consists of two plastic scintillators with a surface area of 40 cm wide by 60 cm high, read out by 5 cm diameter, magnetically shielded photomultiplier tubes (PMT). The PMT counts, including various measurements of coincidence among the four scintillator paddles, are recorded by the ALPHA detector data acquisition system. Data from the scintillators can be used to monitor antiproton annihilation to extract quantities such as the total number of trapped antiprotons, their plasma energy distributions, and annihilation rates on the background gas.

3.2. The positron accumulator

The Positron Accumulator used in ALPHA-2 is the same device that was previously used in ALPHA-1; this is shown in Fig. 10 and has been described in detail elsewhere [11,12]. Techniques based upon the buffer gas accumulation methods pioneered by Surko and colleagues [50,70] can routinely collect $3\text{-}4 \times 10^7$ positrons within the apparatus after 200 s admittance of a continuous, low energy, positron beam.
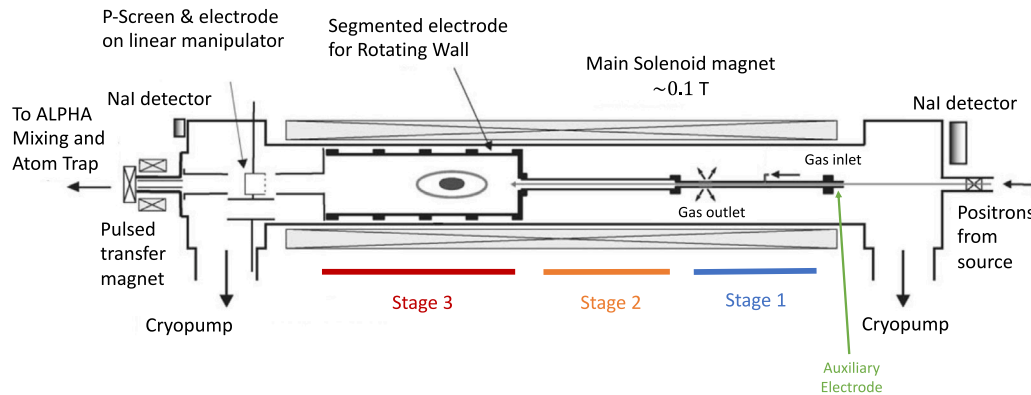
Fig. 10. Schematic illustration of the ALPHA-2 Positron Accumulator. Positrons enter from the beamline to the right and, once the accumulation cycle is complete, are ejected from the third, large diameter stage towards the main antihydrogen production and trapping region. A phosphor screen (viewed by an external camera, not shown) mounted on a linear manipulator can be used as a diagnostic of the transmitted positron beam and the ejected cloud.

Table 1
Parameters of the Positron Accumulator Stages. Bias voltages are occasionally updated to accommodate different operating conditions. ID refers to the electrode inner diameter.

Stage	Length	Electrode ID	Typical Bias	Pressure
aux. elec.	21 mm	12.7 mm	45 V	not monitored
1	509.6 mm	12.7 mm	40 V	1×10^{-3} mbar
2	540 mm	30 mm	32 V	1×10^{-4} mbar
3	4×154 mm	201 mm	23 V; 340 V	1×10^{-6} mbar

3.2.1. Source and moderator

The beam is generated using a commercial system, supplied by First Point Scientific, which harnesses an approximately 0.55 GBq (at the time of writing) ^{22}Na radioactive source, a 4.2 K GM cryocooler and a solid neon moderator [71,72]. High purity (> 99.9999%) neon gas is directed onto the cooled source at a pressure of around 10^{-3} mbar for 100 s and condenses directly onto the source capsule and an inverted cone. This arrangement moderates a fraction of the emitted β-particles, and for improved efficiency it is held at a temperature of 8 K by a PID controlled cartridge heater. Radial confinement of the emitted low energy positrons is provided by a solenoid-generated magnetic field of 35–40 mT. Positrons are accelerated and directed towards the accumulator by a 50 V potential applied to the source. The beam intensity can be recorded via a calibrated NaI(Tl) detector located near a gate valve at the entrance to the accumulator (see Fig. 10) which routinely measures $\sim 5 \times 10^6$ e^+s^{-1}, corresponding to a moderation and transport efficiency of approximately 1%, which is more than twice that previously achieved [11,12].

3.2.2. Accumulator

In order to accumulate the number of positrons required for mixing with the trapped antiprotons, the low energy beam is directed into a 0.1 T solenoid, of length 1.5 m and 0.3 m inner diameter, housing a three-stage Penning-Malmberg trap that utilises molecular nitrogen as a buffer gas to trap and cool the positrons. Nitrogen is the gas of choice [73] due to a prominent resonance in the positron-molecular nitrogen electronic excitation cross-section [74] close to the threshold for the positron energy loss reaction,

$$e^+ + N_2 \rightarrow e^+ + N_2^*, \tag{3}$$
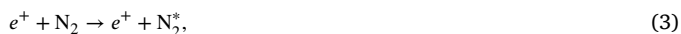
which competes effectively with the usually dominant loss channel, positronium (Ps) formation, as

$$e^+ + N_2 \rightarrow Ps + N_2^+. \tag{4}$$

The Positron Accumulator has three distinct stages, as shown in Fig. 10 and detailed in Table 1. After initially traversing a short auxiliary electrode, the positrons enter the first stage of the accumulator.

Stage 1 is comprised of a single long electrode, designed to introduce molecular nitrogen at mid-length to maintain a pressure of around 1×10^{-3} mbar. This is where the first excitation reactions (Eq. (3)) occur, leading to the first positrons with low enough energy to be trapped. The particles then enter the second stage, which is comprised of a single electrode, which has a larger diameter to aid in maintaining a pressure of approximately 1×10^{-4} mbar. This lower pressure increases the positron lifetime whilst enabling further inelastic interactions with the molecular nitrogen. Following successive collisions, the positrons enter the third stage consisting of four independent electrodes, where a pressure of approximately 1×10^{-6} mbar ensures a lifetime of > 100 s. The first three electrodes of the third stage (including the DC component of the RW electrode) have the lowest voltage (23 V in the example shown in Table 1), whereas the end electrode is held at high voltage (340 V) to provide axial confinement.

Radial transport due to collisions and field asymmetries limit the total number of particles that can be accumulated in the third stage. To counter these undesirable interactions, the first electrode (nearest the second stage) is azimuthally segmented into six pieces enabling the application of the rotating wall (RW) technique [60,75–77] to compress the positrons. Positron clouds containing around 4×10^7 particles within radii of ~ 1.5 mm and at densities of $\sim 5 \times 10^8$ cm^{-3} are readily achieved within 200 s with the continuous application of a 2 MHz, 2 V amplitude, sinusoidal signal applied to each segment, each with a phase difference of $\pi/3$ (to achieve a dipolar field) provided by a custom-built 6-channel arbitrary function generator. The pressure and applied voltages within the accumulator are optimised for the required accumulation time and positron beam energy. Examples of the accumulated number, $N_e(t)$, with time are shown in Fig. 11.

For reasons that are not completely clear, though likely explained by contamination of the neon moderator by N_2 from the accumulator, the flux of low energy positrons decreases with time, with an approximate 20% loss in flux over a period of 10 days. No modification to the accumulation cycle is necessary to mitigate this although the output is commensurately reduced. A new moderator is produced approximately every four weeks by warming the cold head to 35 K and following the aforementioned neon condensation procedure.

Plasma characteristics are monitored by a 50.8 mm diameter P-43 Phosphor screen mounted on a linear translator, (similar to the diagnostic manipulators used elsewhere in ALPHA-2). The images produced enable the positron number and the radial profile to be determined following calibration. In order determine the number, the integrated intensity of light recorded by the CCD is calibrated against the measured charge when the screen is used as a Faraday cup. This is also cross-calibrated independently against a previously calibrated CsI-photodiode detector. In order to deduce the spatial dimensions, reference points on the phosphor screen are compared to their location
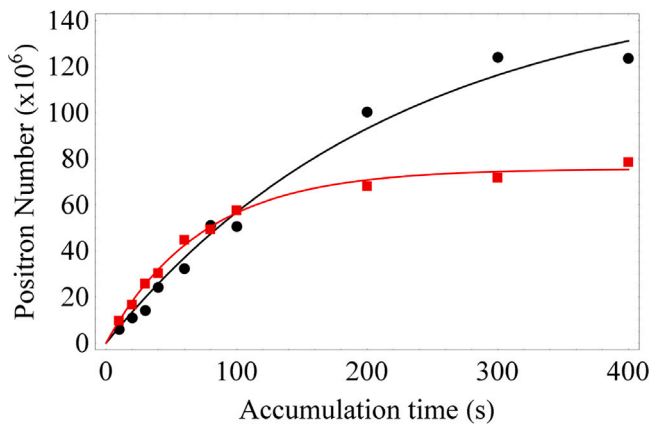
Fig. 11. Accumulated positron number $N_e(t)$ versus accumulation time, t, for nitrogen pressures of 5×10^{-4} mbar (black filled circle) and 1×10^{-3} mbar (red filled square) in the first-stage. The solid lines are fits to the function $N_e(t) = R\tau_e(1 - \exp[-t/\tau_e])$, where R is the accumulation rate and τ_e is the positron lifetime within the apparatus. Accumulation rates of $(7.0 \pm 0.6) \times 10^5$ s^{-1} and $(1.04 \pm 0.04) \times 10^6$ s^{-1}, and lifetimes of (223 ± 35) s and (73 ± 4) s, are obtained at the lower and higher pressures respectively.

within an image when an external light source is used for illumination, and the magnetic field ratio between the trap and measurement point is taken into account. With these calibrations, and using a 2D Gaussian fit to the images, the density can be characterised and operational settings can be optimised.

3.2.3. Positron transfer

Following accumulation, the positrons are prepared for transfer to the Mixing Trap following the procedure used by ATHENA [49]. Since the presence of nitrogen gas is detrimental to the long-time storage of antiprotons (see Section 3.1.2) its admittance into the accumulator is halted and two 1200 Ls^{-1} cryopumps evacuate the accumulator region to 4×10^{-8} mbar in approximately 10 s. During this time, the accumulator voltages are slowly raised to improve the transfer efficiency: transfers starting from higher potentials result in ballistic ejection with higher velocity, which is less likely to suffer from magnetic mirroring losses. A mechanical gate valve isolating the accumulator and the Mixing and Atom Traps is opened for 2 s and a transfer magnet is pulsed to a field of 1 T to facilitate particle transfers through the intermediate region, and to compress the cloud as it traverses a cylindrical aperture. This aperture has an intentionally small cross section to reduce nitrogen gas contamination of the main ALPHA-2 Apparatus. Mobile CsI detectors can be placed at multiple locations around the apparatus to detect photons produced by the annihilation of positrons. These detectors can be used to tune manipulations used in the ballistic ejection procedure in order to maximise the transfer of positrons through the aperture.

Positrons are released and recaptured 3.2 µs later in the Mixing Trap, where they are recompressed and cooled via synchrotron radiation emission. The efficiency of this transfer, compression and cooling sequence is better than 25%. While there is room for improvement in this efficiency, the number of transferred positrons is not yet a limiting factor in overall antihydrogen production rates.

3.3. Mixing trap

3.3.1. Overview

Once antiprotons have been captured and cooled in the Catching Trap they are transferred to the Mixing and Atom Trap region where they will eventually be merged with positrons to form antihydrogen. Fig. 12 details the charged particle Penning trap system used for the final preparation of the antiprotons and positrons as well as for synthesising the anti-atoms. The Atom Trap is co-located in this region; the relationship between the Mixing Trap and the Atom Trap can be

seen in Fig. 16 in Section 3.5.

The preparation and mixing trap system is centred inside an external Main Solenoid magnet that delivers a background field of 1 T. The system has three distinct regions: a central region (electrodes A08–A20) where positron and antiproton mixing occurs, and two side traps which are used for antiproton (A01–A07) and positron (A21–A27) preparation. Superposed on the central region are the superconducting magnets that comprise the trap for antihydrogen atoms. The electrodes in this region have an enlarged internal diameter in order to exploit as much as possible of the atom trap depth, which is determined by the large radial gradient of the magnetic field of the octupole. The design follows that of the original ALPHA apparatus [12], where the excitation is delivered with flexible circuit boards to save radial space and the electrode stack cohesion is maintained with tensioned wires. This radial-space saving strategy is not necessary in the side traps, that have a smaller internal diameter and are assembled using a more traditional external skeleton structure using threaded rods.

Most of the electrodes in Fig. 12 (A02–A06, A09–A19, A22–A26) have identical length-to-inner-diameter aspect ratios (0.45), optimised to allow the easy formation of harmonic potential wells at any location. The lengths of these two types of electrodes are 13.22 mm for the side traps and 20.05 mm for the inner section. The electrodes which do not conform to this aspect ratio, namely the end and transition electrodes, have dimensions as specified.

The antiproton and positron side traps have superposed short solenoids to boost the field to 3 T during particle preparation. Fig. 12 shows the axial magnetic field in the two traps when energising solenoid A (left) and solenoid B (right) respectively. The higher field in these regions primarily serves to help plasmas cool faster by increasing the rate of cyclotron radiation energy loss.

The trap system is heat-sunk to the cryostat helium volume through a copper feedthrough mounted at a radial step in the vacuum chamber to the right of the components shown in Fig. 12. The electrodes are electrically, and thus also somewhat thermally, insulated from each other by ruby balls that also serve to locate electrodes co-axially. Therefore, additional thermal heat-sinking is provided to the electrodes by clamping the flexible circuit board to the heat-sink. The trap temperatures are monitored with Cernox sensors clamped to A02, A20, and A26 and at equilibrium these electrodes settle to temperatures between 6.5 and 6.9 K.

3.3.2. Electrical signals and connections

The electrodes are individually controlled from an FPGA-based system where signals in the ±10 V range are amplified through custom-built electronic devices that were used previously both in ALPHA and ATHENA. The signals to the electrodes pass through a filtering system at the feedthrough into the vacuum system: each electrode has both a low-pass filtered input and a high-pass filtered input. The low-pass input is used for steady voltages and has a cut-off around 200 kHz. This is similar to the trap connection instrumentation used in the Catching Trap, as described in Section 3.1.5. The amplifiers allow the excitation of the majority of the electrodes in the range ±140 V, with a time-constant of about 2 µs. The amplifiers for the electrodes that are directly involved in the merger of positrons and antiprotons (A10–A15) have been modified to be further filtered to reduce electronic noise. For these, the output range is reduced to ±75 V and with a time-constant of 0.1 ms.

The end electrodes A01 and A27 operate as gate electrodes for the transfer of, respectively, antiprotons and positrons that are ballistically transported from the Catching Trap and Positron Accumulator. They are each connected without filtering to fast switches that have rise-times of around 10 ns.

The high-pass filtered input is used for fast signals including rotating wall drives, e-kick pulses, plasma-mode excitation and detection, and auto-resonant drive. These uses are described in more detail below.
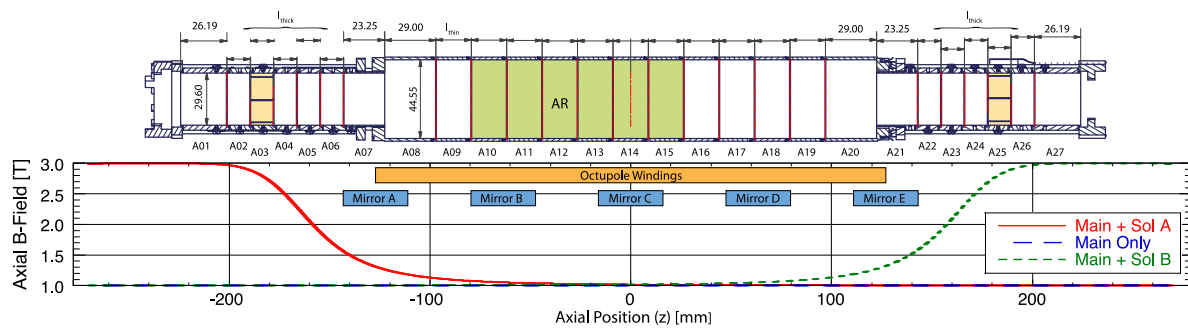
Fig. 12. Detail of the Mixing Trap electrodes. The ALPHA-2 Mixing Trap system consists of 27 cylindrical electrodes that can be individually biased. The Atom Trap is superposed on the central 13-electrode (A08 to A20) arrangement, and here the inner diameter is enlarged to 44.55 mm to enhance antihydrogen trapping. The inner diameter of the enclosing vacuum chamber is 48.00 mm. The two side traps have inner diameters of 29.60 mm and are used for preparing antiprotons (left side) and positrons (right side) for mixing. Two electrodes (A03 and A25 in yellow) are six-way azimuthally segmented for application of rotating wall drives, and 6 electrodes (A10–A15 in green) are excited by heavily filtered amplifiers to reduce electronic noise. The lower pane shows the axial magnetic field in this region.

Rotating wall: The two azimuthally segmented electrodes (A03 and A25) each have segments connected in parallel through the low-pass connection to a single output on an amplifier to provide a DC offset, while the segments are connected individually through six high-pass connections. A six-way custom built function generator, which can accommodate arbitrary phase-shifts between the channels, is used to deliver dipolar or quadrupolar rotating wall drives in either the clockwise or anti-clockwise direction. The rotating wall drive amplitude can be varied in the range (0.2–20) V, with the frequency variable between 10 Hz and 30 MHz, though impedance mismatches in the connection chain from the driver to the electrodes restricts the consistent response range to below about 10 MHz.

e-kick: Fast pulsers are available for extracting electrons in a process called e-kicking. A voltage is briefly applied to an electrode which causes the electrons to be ejected, but the voltage is removed quickly so that antiprotons (which respond more slowly due to their higher mass) remain trapped. The e-kick pulsers can deliver square pulses between 20 ns and 1 μs in length with a rise/fall-time of about 10 ns. They are normally connected through the high-pass connection to the electrodes.

Plasma modes: A nondestructive magnetic field diagnostic can be created by connecting a drive signal and pickup signal to (the high-pass connection of) electrodes on either side of a confined plasma. Such a system can be used to excite and measure the quadrupole mode frequency of the plasma, which is used as a proxy measurement for plasma temperature. By observing how this mode frequency changes when microwaves are injected to excite electron cyclotron resonance (ECR) heating, the static magnetic field can be deduced [78]. When measuring the central field on axis in the middle of the Atom Trap (i.e., the field relevant for antihydrogen spectroscopy) the plasma is held in A13–A15, with the drive (an arbitrary function generator) connected to A13 and the pickup (a low-noise amplification circuit) connected to A15.

Autoresonance: Injection of antiprotons has sometimes been achieved using autoresonance [79]. This makes use of an arbitrary function generator connected to the high-pass connection for A12 (when the antiprotons are held in A13 and positrons in A14).

Advanced manipulation techniques: Both the plasma modes and autoresonance techniques have now been supplanted by advanced techniques for manipulating plasmas with finely-tuned electrode voltage sequences. With the advent of a new method for plasma stabilisation [61], a gentle merging of plasmas was observed to produce more trappable antihydrogen than autoresonance. Plasma modes measurements have been replaced by "scooping" tiny plasmas from a reservoir to perform destructive ECR measurements; this has the advantage that the tiny plasma (which is too small to support a modes measurement) results in a highly localised measurement of the magnetic field.

3.3.3. Diagnostic manipulators

The Mixing Trap has two diagnostic manipulators (or "sticks"), shown in Fig. 13, one on each end of the Mixing and Atom Trap. Similar to the diagnostic manipulator of the Catching Trap (described in Section 3.1.6), these sticks are used for particle loading and plasma measurements. The sticks are interchangeable, and each stick is outfitted with a passthrough electrode, two electron guns, two MCP's, and two Faraday cups.

The passthrough electrode can be biased up to 5 kV to aid in particle transport between traps. These are made of aluminum (to reduce weight) that is gold-plated (to reduce outgassing) using a copper strike. They are held in place by a PEEK jacket for electrical insulation.

The electron guns use a Barium Oxide cathode and electrically biased plates to produce a beam of electrons for injection into the particle traps. The Faraday cups consist of a plate of 316LN stainless steel, with a capacitance measured *in situ*.

Each MCP (part number 38074 from Photonis, USA) is 40 mm in diameter and is paired with a P46 phosphor screen. The image is reflected by a ThorLabs E02 dielectric-coated mirror, and recorded by a CCD camera.

The temperature component parallel to the direction of ejection can be measured using either the Faraday cup or by measuring the (amplified) charge deposited on the MCP via Eggleston's method [80].

3.4. Preparation of antimatter plasmas

In order to produce antihydrogen, positrons and antiprotons must be carefully mixed. A basic optimisation strategy for producing the anti-atom is to prepare positron and antiproton plasmas that are cold and dense. Higher densities are desirable because this increases the probability of particles interacting, until the point where electric fields inhibit antihydrogen formation [9,81]. Recombination rates are observed to be highest when positron temperatures are low [16], and low antiproton temperature leads to more trappable (low energy) antihydrogen atoms because the antiprotons carry most of the momentum of the nascent antihydrogen [82].

Experimentally, clear correlations have been observed between temperature decreases and increased antihydrogen formation and trapping rates, though the production rate benefits saturate at a point before antiproton temperature and density reach their experimentally achievable extreme values. This may be due to geometric and non-equilibrium effects that are not captured by simple scaling models, though systematic studies have not yet been conducted.

The ALPHA-2 apparatus has the capability to energise and de-energise magnets to optimise particle manipulations. However, experiments have shown that the particle manipulations can also be performed even when all of the Atom Trap magnets are energised, leading to the experimentally advantageous ability to accumulate antihydrogen over multiple mixing cycles [16]. When experiment protocols
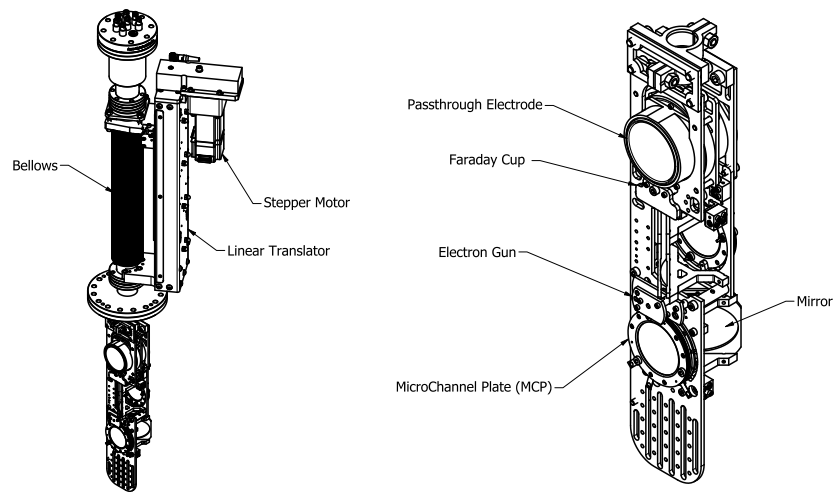
Fig. 13. Diagnostic manipulators for the Mixing Trap. Left: Rendering of the (internal) diagnostic array attached to the (external) linear translator via bellows. Right: A closer view of the diagnostic array which includes a passthrough electrode, an electron gun, an MCP, and a Faraday Cup plate. Another Faraday Cup, electron gun, and MCP are mounted on the back.

call for the sudden release of trapped antihydrogen, the Atom Trap magnets can be de-energised in 1.5 s.

3.4.1. Preparation of antiprotons

The antiprotons are received from the CERN AD complex in the Catching Trap, where they are cooled and compressed sympathetically with electrons [46]. After the final cooling, where about 10^5 electrons are used to cool a similar number of antiprotons, the electrons are removed by applying a fast-pulsed electric field (an e-kick, see Section 3.3.2).

The antiprotons are then transferred (making use of the transfer magnet system described in Section 3.7) across into their preparation section of the Mixing Trap (electrodes A01–A07 in Fig. 12). This subsection of the Mixing Trap is called the re-catching trap. Before the transfer, antiprotons (typically with a temperature around 300 K) are loaded into the pre-transfer well shown in Fig. 14 (left pane), while electrons are loaded into the re-catching trap 3 m downstream, and are located in the pre-transfer potential shown in Fig. 14 (right pane). The Catching Trap potential is then changed in one control step to the post-transfer potential, and the circuit response is such that this change happens in about 2 μs. The re-catching trap gate electrode (A01) is, after delay of 50.6 μs, excited in about 10 ns to achieve the post-transfer potential in Fig. 14. This coordinated transfer procedure results in the capture of the $\bar{p}$s in the re-catching trap; by appropriate tuning of the delay we find that 100% of the antiprotons can be recaptured.

Particle manipulations that occur after this coordinated transfer are independent of the Catching Trap, and thus are decoupled from the timing of the AD beam cycle. Once in the re-catching trap, antiprotons go through another cycle of sympathetic manipulations with electrons: antiprotons are cooled and compressed, and then the electrons are ejected using the e-kick (fast pulser) procedure. Prior to mixing with positrons, there are typically around 10^5 antiprotons at a temperature of about $T = 100$ K and a radial extent of about $r = 1.5$ mm, though colder and denser plasmas can be achieved ($T \lesssim 20$ K, $r \sim 0.4$ mm) by applying further evaporative cooling [47].

3.4.2. Preparation of positrons

Positrons are collected and manipulated in a dedicated positron accumulator, which is discussed in Section 3.2 and has been previously described elsewhere [12]. Like the other charged particle traps in ALPHA, the positron accumulator uses an axial magnetic field and cylindrical electrodes to trap and manipulate positrons. Unique to the positron accumulator, this trap also features deliberately introduced

nitrogen gas, which is differentially pumped to sustain a pressure gradient across the trap. Although some positrons are lost via annihilation, this environment enables a large number of positrons to cool through scattering collisions with the nitrogen. The net procedure yields a plasma containing hundreds of millions of cool positrons in the positron accumulator.

In a process analogous to the transfer of antiprotons to the Mixing Trap, positrons are ballistically transferred to the Main ALPHA-2 apparatus using electrode A27 as a fast gate for dynamic trapping. (More details of this process are described in Section 3.2.3). The incoming positrons are cooled into a well in A14–A15 and then adiabatically transferred to a well underneath solenoid B. Prior to further operations, a radio frequency heating drive is applied to remove trapped positive ions that are created during the transfer. The presence of ions has been observed to cause the positrons to heat and thereby prevent efficient rotating wall compression.

Following the ion clearing process the positrons are post-processed using a combination of strong drive RW and evaporative cooling; the combined process is called SDREVC [61]. This combination secures reproducible and controllable initial conditions for the positrons before mixing. Prior to the discovery and implementation of the SDREVC technique, fluctuations in the accumulation or transfer efficiencies directly impacted the antihydrogen synthesis process, making systematic studies difficult and ultimately causing sub-optimal anti-atom trapping efficiencies. This technique, in which the application of strong drive RW and evaporative cooling are simultaneously applied, fixes both the density and volume occupied by the plasma, thereby also determining the number of particles.

Following this process, and depending on the final positron density desired, further RW compression may be applied. Finally, the positrons are adiabatically transferred to a pre-mixing potential well in A14. Typically we prepare several million positrons with a density of around 10^{14} m^{-3} and radius of 0.44 mm at a temperature of about 50 K.

3.4.3. Mixing of antiprotons and positrons

The Atom Trap is formed by energising the octupole and at least two mirror coils around the synthesis region. This can be accomplished in 18 s (limited mainly by the ramp-rate of the octupole magnet) after particles have been prepared for mixing. However, more recent tests have shown that particles can be fully prepared with the Atom Trap magnets energised in a steady-state. This mode of operation allows for antihydrogen accumulation through stacking [16].

With the Atom Trap magnets energised, the positrons are evaporatively cooled again using the SDREVC method, then mixed with the antiprotons to form antihydrogen. Different methods of mixing have been
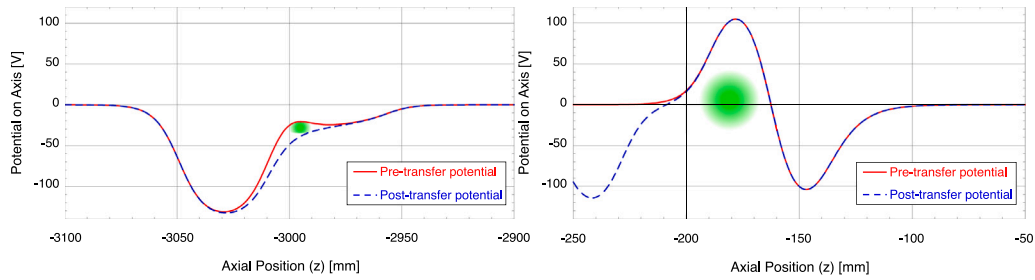
Fig. 14. Electric potentials on axis in the Catching (left) and re-catching (right) traps for the transfer of antiprotons. The axial positions are absolute relative to the centre of the Mixing Trap (A14). The re-catching trap potential change, effected by a fast gate, is applied at a delayed time relative to the change in the Catching Trap. Representative charged particle clouds (in green) indicate the nominal position of trapped antiprotons before (left) and after (right) the transfer.
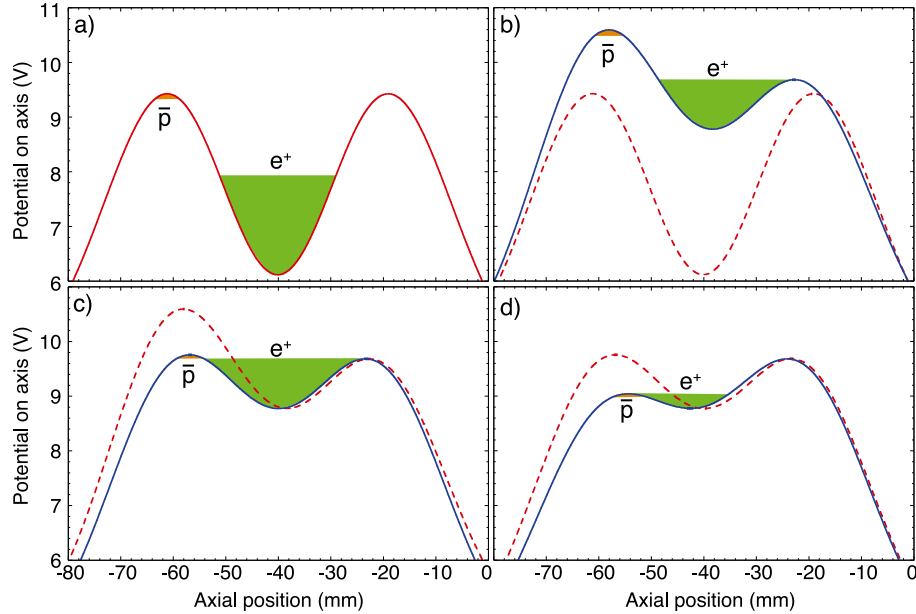

Fig. 15. Electrode potentials in the Atom Trap region when mixing positrons and antiprotons. The curves represent the electrostatic potential before (dashed) and after (solid) each step of the manipulation: (a) The potential before evaporative cooling; (b) evaporative cooling during which positrons escape to the right; (c) preparation for mixing (duration 10 ms); (d) Potential merge mixing (duration 1s). Positrons escape to the left during mixing, resulting in further evaporative cooling. After mixing is complete, any remaining positrons are ejected to the right while any remaining antiprotons are ejected to the left.

tested, including the injection of antiprotons using autoresonance [79, 82] and various manipulations of the confining potentials.

A successful mixing sequence (which does not use autoresonance injection) is shown in Fig. 15. Particles are prepared in the wells shown, and mixing occurs when the positrons are very carefully allowed to spill out of their well to interact with antiprotons.

3.5. The atom trap

The Atom Trap is designed to produce a magnetic field with a central minimum in $|\vec{B}|$, as shown in Fig. 16. Atoms with a low enough kinetic energy (less than about 0.5 K equivalent) are confined in this field by the interaction between the applied field and the magnetic dipole moment of the atom. This interaction can be characterised by the potential energy function $U = -\vec{\mu} \cdot \vec{B}$.

The inner ALPHA-2 magnet system consists of two solenoids (denoted A and B in Fig. 16) positioned symmetrically at both ends of the system, an octupole spanning the central space, and five short, equally spaced solenoid-like mirror coils (labelled A-E in Fig. 16). The centre-to-centre span of mirrors A through E is 274 mm, for a mirror separation distance of 68.5 mm. These coils overlap the axial length of the octupole, and occupy a higher radius, as shown.

All windings are fabricated with low temperature superconducting NbTi cables formed by surrounding six wires around a central one.

All seven wires are identical, and are manufactured by Supercon Inc (model SC-56S53-0.33 mm). The wire measures 0.30 mm in diameter uninsulated. The NbTi within each wire is distributed in 56 filaments, each measuring 30 μm in diameter, embedded in a copper matrix. The copper-to-NbTi ratio is 0.9:1, which is low compared to typical magnet conductors, in order to maximise current capacity. The standalone wire is measured to carry a critical current of 147 A in a 3 T background field in short sample tests. After cabling, the 6-round-1 bundle is wrapped helically in Kapton strip (with 50% overlap) for electrical insulation. The assembled wire bundle measures 1.1 mm in diameter.

None of the windings are built to enable a persistent mode of operation; current in all windings always pass through the external power circuit. This design choice was made to allow the magnets to be ramped (changed in current) often during operation. Frequent ramping implies that any persistent mode would require frequent toggling, which is typically accomplished through the use of a persistent-mode switch (an element which can be heated or cooled to move between normal-conducting and superconducting). Frequent use of a persistent-mode switch would have negated the cryogen-saving advantage of persistent operation.

Current from the power supplies is delivered to the cryogenic windings through eight pairs of 500 A hybrid current leads designed and fabricated by CERN. (The leads can be operated at up to 950 A, despite the 500 A rating.) Each contains a vapour-cooled-lead (VCL) section
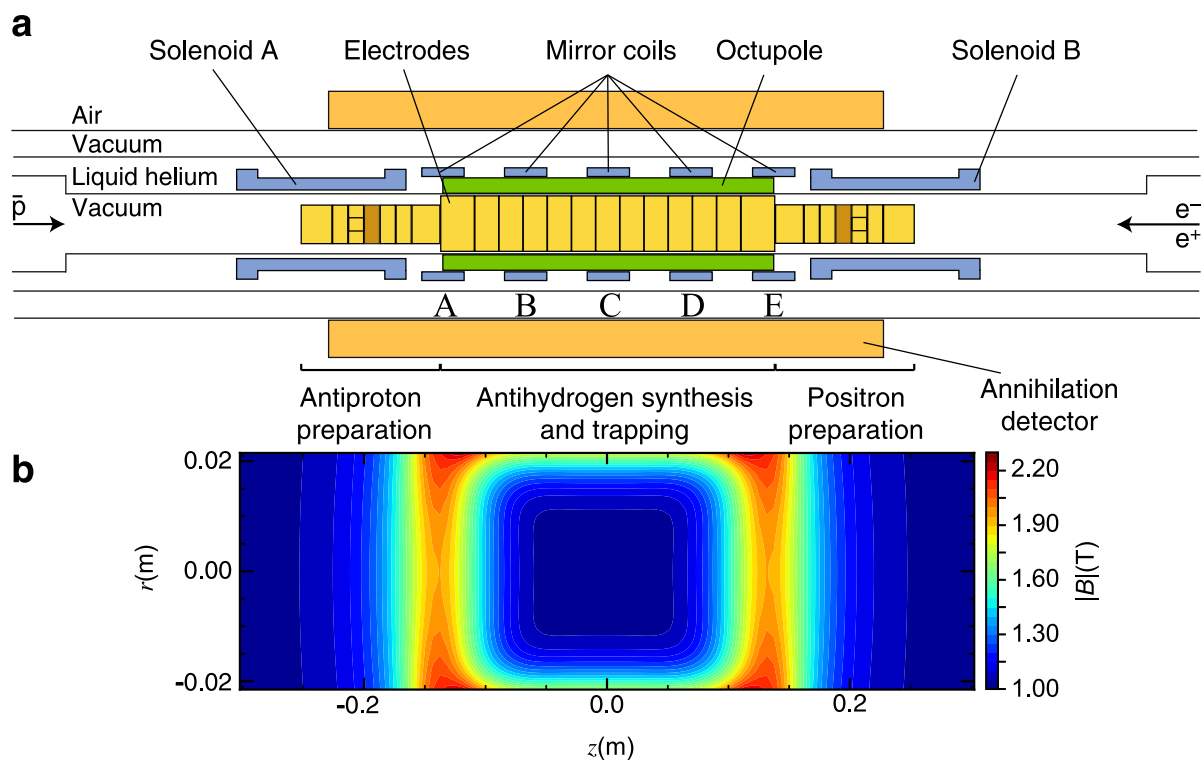
a

b

Fig. 16. (a) Schematic of the central portion of the Atom and Mixing Trap apparatus. The electrodes, together with a ~1 T background magnetic field, comprise the Mixing Trap which is used for charged particle manipulation. In the same physical location, the octupole and mirror coils comprise the Atom Trap, which forms a magnetic field capable of trapping a subset of the atoms that are created. (b) The magnetic field structure forms a minimum in $|\vec{B}|$. Atoms with energy equivalent less than about 0.5 K are confined in this field due to the interaction between their magnetic dipole moment and the magnetic field, which has potential energy $U = -\vec{\mu} \cdot \vec{B}$.

which conducts current from room temperature to 20 K, and a high temperature superconducting (HTS) section which conducts the current from 20 K to 4 K. The cooling vapour is supplied by the boiling liquid helium of the inner cryostat, which is siphoned from above the cryostat's liquid level and passed into the leads. The flow rate in each lead is regulated by a PID controller, which maintains the temperature of the VCL-HTS junction at 20 K regardless of the changing resistive heat load in the VCL during experiments. The HTS section allows the cold end of the VCL to be maintained at a higher temperature, reducing the required flow of boiled-off gas. The HTS section also drastically lowers the heat load on liquid helium, as the HTS conductor has minimal thermal conductivity relative to the normal conductor within the VCL. See Section 3.6 for more details on the cryogenics.

3.5.1. Solenoids and coils

The solenoids depicted in Fig. 16 are 141 mm long and have an inner diameter of 56 mm. Each solenoid consists of three coil blocks - a base block of 8 layers × 122 turns covering the whole solenoid length, and two shape blocks of 6 layers × 16 turns on both ends of the solenoid built on top of the base block. Each solenoid can generate a maximum axial field of 2 T at 238 A, which boosts the uniform 1 T background to 3 T. This stronger field is used during plasma preparation (see Section 3.3) to enhance the rate of energy loss for electron and positron plasmas through emission of cyclotron radiation. Electron cooling improves the antiproton catching and cooling efficiency; positron cooling is necessary for efficient antihydrogen production.

The five mirror coils are 34.68 mm long and have an inner diameter of 82.5 mm. Each coil contains 4 layers × 30 turns, and is capable of generating a maximum field of 1.2 T in its centre at 750 A on top of a 1 T uniform background field. The mirror coils are used to provide axial confinement to antihydrogen atoms, and to shape the axial field profile seen by the anti-atoms and improve spectroscopy precision for lines sensitive to magnetic field strength.

Both the solenoids and the mirror coils are fabricated layer-by-layer in a radial buildup process developed at Brookhaven National Laboratory (BNL). At the start of a winding, a layer is formed by winding the conductor cable in a helical pattern on a wet Stycast 2850FT epoxy substrate. Both ends of the conductor are lifted from the cylindrical winding surface outside of the helical pattern and remain unbroken. One end is routed through a pre-machined groove in the bobbin and serves as the in-current lead of the winding. The other end serves as the starting point for the next layer. This minimises the need for superconductor joints (splices). Additional epoxy is applied on top of the helical winding to encase it, with a small thickness over the top of the conductor to act as the substrate for the next layer. This results in a net layer thickness of 1.24 mm. This process is repeated until all layers are completed. The conductor is routed out of the winding after the end of the last layer to serve as the out-current lead. The outer surface of the winding is then wrapped with pre-tensioned glass fibre cloth and epoxy to counter the outward magnetic force when the winding is energised.

To protect the solenoids and coils from quenches, the voltages at three points of each winding are monitored: at the in-current lead, at the midpoint of the coil, and at the out-current lead. During steady state operation, there is no potential difference between the three points on a winding. While powering on (or off) either the winding itself or any other neighbouring windings, the induced voltage differences between points are proportional to one another, since the flux linked by half of the turns of the winding is (almost) identical to those linked by the other half. When a quench occurs, a resistive voltage spike is seen across the two points sandwiching the quenching region, but not in the other section. This signature is detected by a real-time quench protection system, which triggers a solid state switch on the air side that disconnects the power supply and shorts the winding onto a power resistor. This protects the power supply unit, and drains the magnetic energy from the winding before excessive heat is deposited into the quenched region.
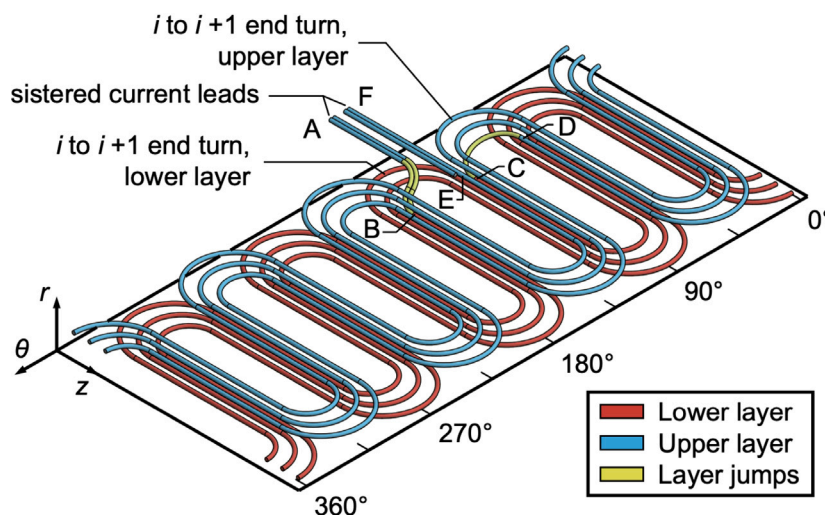
Fig. 17. Layout of the serpentine structure of the ALPHA-2 octupole coil. Note the cylindrical (r, θ, z) coordinate system. See text for details.

3.5.2. Octupole

The octupole occupies the central 280 mm section of the system, and has an inner diameter of 50.8 mm. At the maximum 950 A, the octupole produces a 1.6 T field on the cylindrical wall of the electrodes (r = 22.2 mm). Since this field is perpendicular to the 1 T uniform background field, the net field strength on the wall is 1.89 T, which presents a 0.89 T radial confinement barrier to anti-atoms in the magnetic minimum trap.

Structurally, the octupole is a serpentine multipole made of four bi-layers, the geometry of each is shown schematically in Fig. 17. In this serpentine pattern, an octupole field is generated by eight straight conductor bundles distributed evenly in azimuth, carrying current in alternating directions. The straight segments are connected through semicircular end-turns, which create a continuous conduction path for the entire bi-layer. The end-turns of the lower layer all carry current in one azimuthal sense, which is (mostly) cancelled by the end-turns on the upper layer carrying current in the opposite azimuthal sense. This cancellation is not perfect, as the two layers are at different radii, resulting in a field perturbation on axis that is about three orders of magnitude smaller than the unperturbed octupole field.

The bi-layer shown in Fig. 17 consists of three turns per layer for visualisation purposes. The four actual octupole bi-layers contain more turns to maximise the octupole field. The number of turns that can fit onto a bi-layer is determined by three factors: the cylindrical surface area available to the bi-layer, the minimum separation between conductors within a bundle, and the minimum separation between conductors in two neighbouring bundles. The first is simply proportional to the layer radius. The second is a direct result of the thickness of the conductor, as well as the limitation of the wire placement process. For the conductor and process used in ALPHA-2, the spacing cannot be smaller than ~ 1.24 mm. The third is constrained by the minimum bending radius of the conductor, as the separation between two bundles determines how tightly the innermost end turn can be made without damaging the conductor. This limits the separation between two bundles to be no less than ~ 3.96 mm. Taking these into consideration, the four bi-layers in the ALPHA-2 octupole contain 11, 13, 15 and 15 turns per layer respectively.

The four bi-layers are fabricated using the direct wind method developed by BNL. This process is capable of creating arbitrary winding patterns on a cylindrical surface, by paying out conductor and affixing it onto an epoxy-wetted surface with a stylus vibrating at ultrasonic frequencies. The axial, radial and azimuthal path of the stylus, as well as its wire-paying direction, are computer controlled. Each bi-layer begins where the stylus starts drawing the serpentine lower layer, from point B in Fig. 17. A length of conductor is left un-affixed prior to point

B, to be manipulated later. The lower layer is complete when the stylus reaches point C. Following this, the empty spaces between wires are filled with patches of glass fibre cloth, and the whole lower layer is encased in epoxy. This leaves a smooth cylindrical surface for the upper layer, which is penetrated only by the conductor prior to point B and after point C, both of which are routed to the upper layer. The direct wind machine then resumes winding from point D onward, until it reaches point E. The A-B segment is then affixed (by hand) to the upper layer next to the E-F segment, and both are routed to exit the winding axially. The two serve as the in- and out-current leads for the bi-layer. Both leads are "sistered", i.e. an additional conductor is soldered parallel to each, in order to boost the current capacity in the leads and prevent quenches from happening within them. This is important as the leads experience a weaker magnetic field than conductors within the winding. If a quench occurs within the lead, its propagation along the conductor would be much slower compared to one within the winding. This means the magnetic energy is deposited in a much smaller volume, making a conductor fusing more likely. After sistering, the spaces in the upper layer are similarly filled and epoxy applied, leaving a smooth, unpunctuated cylindrical surface. A bi-layer fabricated this way has a thickness of ~ 2.95 mm.

After the first bi-layer, the second is constructed immediately on top, but rotated azimuthally by 90 degrees. This serves to distribute the leads in azimuthal angle, and simplifies the electrical connections between bi-layers. After the second bi-layer, pre-tensioned glass fibre cloth and epoxy are applied to counteract magnetic forces when the winding is energised, which adds ~ 0.5 mm of radial build-up. After this, the third and fourth bi-layers are constructed, each further rotated by 90 degrees relative to the layer below. Another pre-tensioned glass fibre cloth and epoxy are applied on top of the fourth bi-layer.

The four bi-layers are then connected in series, by splicing the out-current lead of one bi-layer to the in-current lead of the next. These splices are formed by stripping the insulation from ~ 25 mm of the ends of the two conductors, carefully cleaning the surface, overlapping the two ends in parallel (such that current does not have to make a 180 degree turn within the splice), mechanically compressing the ends together, then soldering the overlap together quickly to prevent overheating the NbTi. These splices are physically located immediately next to the axial end of the octupole where the leads exit the winding, and are potted into place with epoxy to constrain against movement caused by magnetic forces. The in-current lead of the first bi-layer and the out-current lead of the fourth bi-layer, which remain free, become the leads for the whole octupole.

As the current has to traverse copper and solder between the NbTi cores of the two conductors in a splice, the joint necessarily has a

small resistance. Quench detection for the octupole needs to be able to exclude this innate resistance in order to identify real quenches, so the voltage in the octupole winding is monitored at eight points: two at the in- and out-current lead of the whole octupole, and two across each of the three splices. The quench detection system is then programmed to monitor for disproportional changes to voltage differences between electrically adjacent points on the superconductor; measurements that cross the splices are interpreted differently from measurements that do not.

3.5.3. Mechanical structure

The windings in ALPHA-2 require strong mechanical supports to counteract substantial magnetic forces. These structures are machined with 316LN stainless steel for its mechanical strength, low susceptibility, crystalline stability at cryogenic temperatures, and high electrical resistivity.

The base structure of the inner magnet system is a cylindrical tube (48 mm inner diameter) separating the ultra-high vacuum bore volume, where experiments take place, from the liquid helium volume in the cryostat. This tube has a central thin-walled section (1.4 mm thick) on which the octupole is directly wound. The thin wall maximises the radial confinement strength afforded to the anti-atoms, but it has to be strong enough to withstand buckling under the radial compression of the octupole tension wrapping. This limits both the thickness and the axial length of the thin-walled section.

After the octupole is fabricated, a concentric tube is slipped over it, on which the mirror coils are wound. This tube is machined with five ring-shaped depressions (bobbins) in which the coils are wound. The depressions provide both radial and axial constraints to the coils, bracing them against the axial attractive magnetic forces between coils and the radial compression from the tension wrapping. The mirror tube does not fit tightly over the octupole, but has a clearance of 1 to 2 mm. It also has large vent windows machined between the bobbins, which allows liquid helium to pass through and cool the octupole directly. The mirror tube is secured onto the octupole tube via two flanges on both ends of the octupole.

The two solenoids are wound on two bobbin tubes, which slip tightly onto the octupole tube after the mirror tube is installed, just outside the flanges. Two nuts are then screwed onto the octupole tube which compress the solenoid bobbins against the flanges, securing them into place.

3.6. Atom and mixing trap cryogenics

During experiment operations, the helium consumption of ALPHA-2 is regularly monitored. On average, the entire system consumes 19 Lh^{-1} of liquid helium during active experiments, as summarised in Table 2; the sources of this consumption are discussed here. Of particular note, however, the overall helium boil off rate is low enough that we must subsidise it with a dedicated heater inside the cryostat in order to generate enough helium gas to operate the vapour cooled leads (introduced in Section 3.5, and discussed further below).

Helium-consuming elements of ALPHA-2 include: (1) a 1000 L dewar; (2) a transfer line from the dewar to the cryostat; (3) the cryostat containing a liquid helium bath; (4) a system of heat shields cooled using gaseous helium vapour flow; (5) a set of actively controlled, vapour-cooled HTS electrical leads and (6) operation-dependent loads. To understand the overall helium consumption of the experiment, we consider each element in greater detail.

By isolating the dewar (1), with the transfer line installed but not in active use, helium consumption was observed to be about 0.4 Lh^{-1}. We can estimate the additional boil-off that occurs when the transfer line (2) is in active use by comparing average consumption during normal operation to that when the transfer line is closed. Use of the transfer line consumes approximately 1.6 Lh^{-1}.

Table 2
Summary of the ALPHA-2 average liquid helium consumption (Lh^{-1}).

1000 L dewar	0.4
Transfer line	1.6
Cryostat and heat shields	9
HTS leads, including internal heater	6.5
Operation dependent sources	1.5
Total	19

The cryostat and heat shields, (3) and (4), have been modelled to give a theoretical baseline consumption of the cryostat. An engineering design analysis predicted two major sources of helium boil-off: (a) that due to heat conduction and radiation, and (b) the supplemental boil-off rate required to maintain the flow of helium vapour. This analysis estimated the rate (a) to be 3.6 Lh^{-1}. If this "natural" boil-off rate was sufficiently high, then the helium vapour produced at the surface of the helium bath could be used to cool the heat shields and baffles to their necessary temperatures. The cold vapour flow requirements, however, correspond to a boil-off rate of 4.4 Lh^{-1}, indicating that a heater must be placed inside the liquid helium bath to provide a supplemental 0.8 Lh^{-1} of boil-off. Thus, the theoretical minimum consumption of the cryostat and heat shields is 4.4 Lh^{-1}.

In an experiment in which the cold cryostat was isolated with cold radiation shields, the minimum cryostat consumption was measured to be approximately 9 Lh^{-1}. With base consumption at this measured level, additional heaters are not necessary to cool the shields (though a supplemental heater is still necessary for normal magnet operations). The significant discrepancy between this measurement and the theoretical minimum consumption is likely due to differences between the modelled ideal cryostat and the cryostat as physically implemented. These differences include heat conduction through the HTS leads, a significant number of signal cables connecting room temperature electronics to sensors in the cryogenic environment, small modifications to the cryostat design implemented after the theoretical estimate was made, and differences between the surface emissivity of the construction materials and our model values. In addition, the cryostat was specifically designed to allow for changes to the internal trap components, so the heat load due to these components changes periodically.

The final significant source of liquid helium consumption, (5), is the HTS lead system. The primary role of these leads is to act as high-current electrical feedthroughs from room temperature into the superconducting magnet wire at 4 K. To maintain the required thermal gradient across them, the room temperature end is actively heated, the cold end is immersed in liquid helium and cold helium vapour flows are actively controlled to maintain intermediate temperatures using PID controllers. The vapour flow required to maintain the HTS lead thermal gradients is larger than the boil-off rate of the cryostat (9 Lh^{-1}), so an internal heater is required. The internal heater is driven by a PID controller and is set up to maintain a user-specified pressure in the helium vapour volume directly above the liquid helium bath.

To maintain operational temperatures in the HTS leads, an additional 6.5 Lh^{-1} of helium boil-off is required. Some of this occurs as a result of the operation of the leads themselves (e.g., heating on the room-temperature end), but is not enough to maintain the required vapour cooling. The rest of the required boil-off is supplied by the internal heater.

In addition to steady state operation, the system is able to respond to additional heat loads during operation. When the superconducting magnets are being cycled, there is an additional load due to Joule heating (in the normal-conducting portion of the HTS leads) and due to superconducting magnet quenching. When this happens, the system detects an increased temperature at the midpoint of the HTS leads, and responds by opening valves to increase helium vapour flow. As helium vapour is used to cool the leads, there is a corresponding drop in helium

gas pressure. This triggers an increase in the internal heater current, which restores the helium pressure to its user-specified value (typically less than 100 mbar above atmosphere). These operation-dependent loads added about 1.5 Lh^{-1} to the overall average consumption.

In general, the instantaneous liquid helium consumption can vary dramatically: the numbers presented in this section are averages over an extended time period (at least several hours). All of the helium used to cool the apparatus is recycled through CERN's helium recovery infrastructure.

3.7. Transfer magnets

The modular concept of ALPHA-2 led to the physical separation of the Catching Trap and the Mixing and Atom Traps, with the distance between the centres of the respective superconducting magnets for these traps being slightly more than 3 m. Due to this separation, further magnets had to be incorporated to facilitate the transfer of charged particles between the traps. These transfer magnets are necessary to prevent particle loss through divergent trajectories in the fringe fields of the superconducting magnets.

Antiprotons are transferred from the Catching Trap to the Mixing and Atom Trap using two transfer magnets operating in steady state. During particle transfer, antiprotons approximately follow magnetic field lines and the beam envelope remains close enough to the beam axis to clear all apertures [83].

Positrons are transferred from the Positron Accumulator to the Mixing and Atom Trap via one steady state magnet and one pulsed magnet. To isolate the relatively poor vacuum in the Positron Accumulator from much the better vacuum condition in the Mixing and Atom Trap, the positrons are transported via a 100 mm long tube incorporating a narrow pumping restriction. To prevent loss of the positrons inside this aperture, a 1 T magnetic field is pulsed for 1 s along the length of this tube, as was previously done in the ALPHA-1 experiment. Once inside the vacuum space of the Mixing and Atom Trap, the positrons are guided by a steady state transfer magnet similar to those used for antiproton transfer.

Two of the transfer magnets (in the region between the Catching and Atom Traps) are identical; a schematic diagram is shown in Fig. 18. The third transfer magnet (between the Positron Accumulator and the Atom Trap) is similarly constructed, but is slightly larger in size. The transfer magnet design was aided by magnetic field and particle trajectory calculations performed using the OPERA finite element field solver [84]. The calculations are estimated to be accurate to 1 part in 10^6 near the axis.

Iron-free construction was required to avoid interference with the fields of the neighbouring solenoids and to have an improved cycle-to-cycle reproducibility. An indirect cooling circuit was added to allow continuous operation.

The cooling circuit is able to remove all the heat produced at peak power, but the thermal gradients inside the coil limit the maximum operating current of the solenoid. This is due to the equivalent thermal conductivity of the coil, which is much lower than that of copper.

The detailed design of the solenoids was performed and documented by the TE-MSC Department at CERN (Technology Department - Magnets, Superconductors and Cryostats) [85,86].

The resulting magnetic field between the traps is shown in Fig. 19(a). An estimate for the beam envelope for an extracted antiproton plasma is shown in Fig. 19(b). This model assumes a confined plasma with initial radius of 1 mm in the uniform field region of the Catching Trap. The plotted envelope assumes the plasma will preserve magnetic flux, but does not account for radial variation in the magnetic field. Under these assumptions, the beam radius $r_b(z)$ will scale as:

$$r_b(z) = r_b(0)\sqrt{\frac{B_0}{B_z(z)}}, \tag{5}$$

where B_0 applies at $z = 0$, which is taken to be the longitudinal centre of the Catching Trap. The envelope shown clears all physical apertures along the beamline.
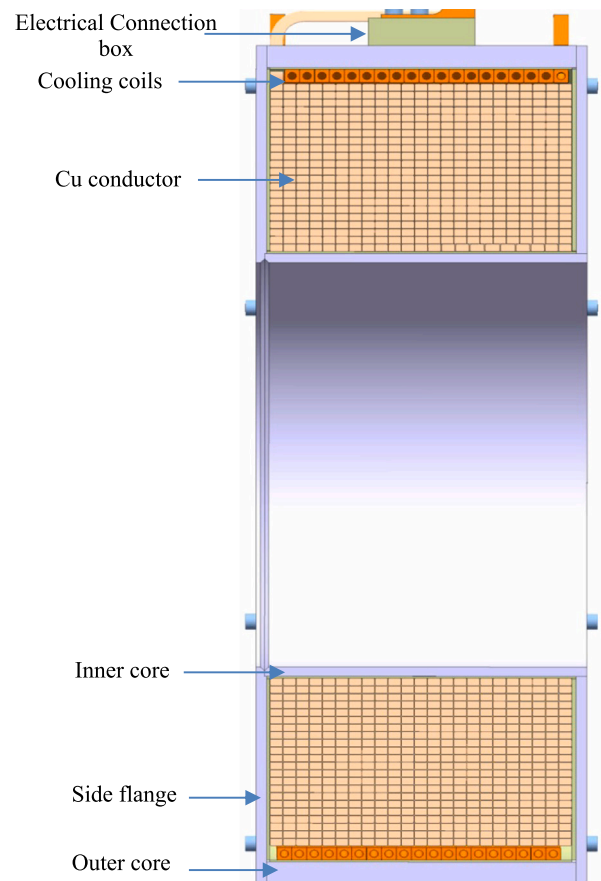

Fig. 18. Cross sections of the Catching to Atom Trap transfer magnets. The magnet produces a maximum field of $B = 0.150$ T, and is used to transfer particles between sections of the ALPHA-2 apparatus. The coil is 140 mm long, with an inner aperture of 110 mm and an outer radius of 250 mm.

3.8. Laser systems and access

The Mixing and Atom Trap has four laser paths which cross the trap axis at an angle of $2.3°$. The lasers can be injected and extracted through windows located at either end of the 3 m long apparatus. Optical tables (enclosed for safety) are secured to both ends of the apparatus to mount the mirrors and detectors necessary for steering and diagnosing the beams. The laser systems are located in a separate laboratory close to the experimental area, which has environmental control and is a designated clean room. The laser beams are transported through enclosed periscopes between the laser laboratory and the optical tables mounted to the apparatus.

Inside the vacuum, each beam enters and leaves the central mixing and atom trap region through one of eight 10-cm long tubular structures that act as *absorptive* broadband microwave filters, developed specifically for the ALPHA-2 apparatus [87]. Laser radiation passes unobstructed through each filter via an 11-mm diameter clear central bore, but K- and Ka-band thermal radiation through the same passage is strongly attenuated by a thin film of Nichrome on the inner surface of an alumina tube. This attenuation, combined with the low radiative temperature of these cryogenic filters aids in the synthesis of cold antihydrogen by helping to minimise unwanted heating of electron and positron plasmas at frequencies of order 28 GHz, where cyclotron resonances occurs in the 1 T base magnetic field of the apparatus.

3.8.1. The 1S-2S laser system

Exciting the $1S$-$2S$ transition requires an enhancement cavity to build up a sufficient intensity of 243 nm light within the Atom trap [88].
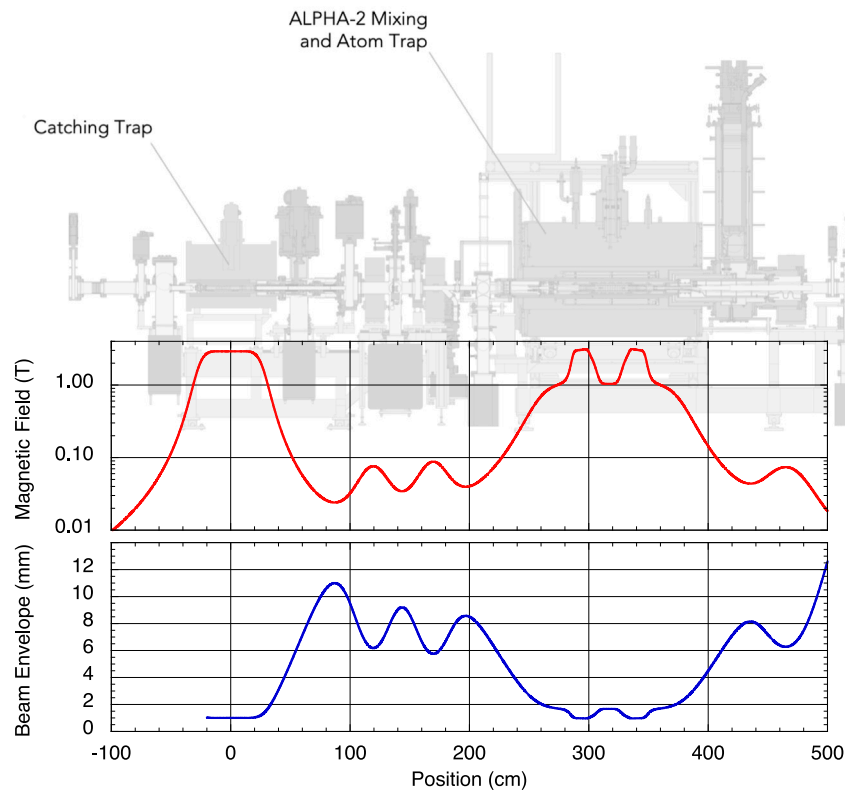
Fig. 19. Top: Plot of the calculated axial magnetic field (B_z) along the beam line and through the Atom Trap at the nominal operating points for the magnets. Bottom: Beam envelope for antiprotons with an initial radius of 1 mm extracted from the centre of the Catching Trap. A silhouette of the apparatus is superimposed for reference.

A schematic of this cavity, along with the rest of our $1S$-$2S$ laser system is shown in Fig. 20. The cavity is formed using two concave mirrors with a radius of curvature of 1 m mounted on either side of the trap magnets with a separation of 90 cm, and in the same UHV region as the antihydrogen trap. The mirrors are pre-assembled in a non-magnetic and low outgassing elastomeric cell [89] or flexure mount [90] to prevent the mirrors deforming or fracturing during the cool down from room temperature to 4 K. These assemblies are installed into triangular shaped mounts which mate with the ends of the magnet form via a 3-point pattern to assure a reproducible alignment of the cavity. Re-alignment of the cavity is not possible once the vacuum system has been closed. The mounting system is depicted in Fig. 21.

The beam waist of the cavity is 0.196 mm, and a circulating power of approximately 1 W is achieved, giving a peak intensity of approximately 1650 Wcm^{-2} in the centre of the trap. The input mirror has a nominal reflectivity of 99% and the output mirror has a nominal reflectivity of 99.5%, giving a theoretical finesse of 417 and a theoretical enhancement factor (defined as the circulating power within the cavity divided by the input laser power) of 132. In practise, a finesse of 250 is measured and an enhancement factor of around 30 is achieved, limited by degradation of the cavity mirrors. The output mirror is mounted on a piezoelectric actuator which is used to lock the cavity length to the laser frequency. The error signal used to lock the cavity is generated using the Pound-Drever-Hall (PDH) scheme [91], and a PID controller (Toptica Digilock 110) feeds back on the piezo via an amplifier (PiezoDrive PX200) to lock the cavity to the laser frequency.

A Toptica FHG-pro laser is used to generate 140 mW (typically) of 243 nm light by amplifying the output of a 972 nm external cavity diode laser (ECDL) and frequency doubling the light in two stages. The beam is collimated using a pair of cylindrical lenses and mode-matched to the enhancement cavity using a Galilean telescope. An electro-optic modulator (EOM) imposes 6.25 MHz sidebands on the

243 nm beam for use in the aforementioned PDH locking scheme. The beam is sent though an enclosed periscope to the optical table on the upstream side of the Atom and Mixing Trap along a 6 m path. The beam pointing is stabilised on the optical table using two position sensitive detectors paired with piezo-actuated steering mirrors. Of the 140 mW laser output, more than 40 mW is injected into the cavity. Losses occur due to damage in the optical elements and due to chemical effects in the air. The air-losses are most significant in the enclosed path between the laser laboratory and the apparatus, as the optical path is otherwise "stirred" by the air conditioning system, and these have been partially mitigated by flowing dry N$_2$ gas through the path between the laser laboratory wall and the apparatus. The optical damage is most significant in the laser access window and the input mirror substrate where the beam waist is at its smallest, and losses in these optics of up to 50% have been measured at the end of a $1S$-$2S$ spectroscopy campaign. These are also the most time-consuming components to replace, as they require airing up the apparatus.

The frequency of the 972 nm ECDL is stabilised by locking it to an ultra-stable reference cavity (based on Menlo Systems ORS 1500). An acousto-optic modulator (AOM) is used in double-pass configuration to shift the light from the $1S$-$2S$ transition frequency to the closest resonance of the reference cavity, and a PDH feedback loop is used to lock the laser to the cavity. The feedback loop corrects the high frequency fluctuations by acting on the diode current, and corrects the long term drifts by acting on a piezo behind the grating of the ECDL. A femtosecond frequency comb (Menlo Systems) is used to monitor the frequency of the reference cavity resonance, and relate it to the SI second using a GPS-disciplined quartz oscillator (K+K Messtechnik). A beat note is generated between the GPS-disciplined oscillator and a thermal caesium clock (Symmetricon CS4000), and the count reaches a fractional Allan Deviation of 8×10^{-13} after 1000 s of averaging. This enables a conservative estimate of the average absolute laser frequency during the $1S$-$2S$ spectroscopy excitation period with 250 Hz precision
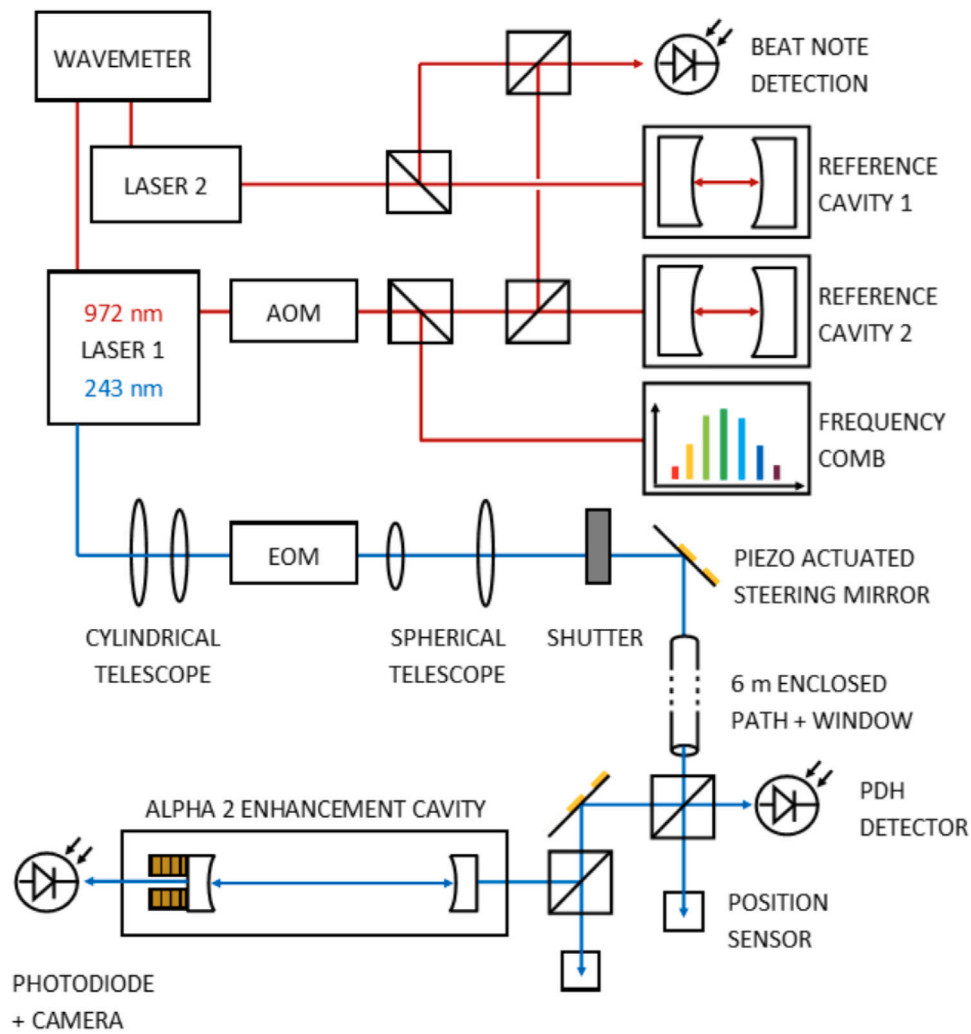
Fig. 20. Schematic of the 1S-2S laser system. A 972 nm external cavity diode laser (ECDL) is carefully measured and tuned, then frequency doubled twice. The resulting 243 nm light is delivered to the Mixing and Atom Trap, where the intensity is increased by the internal enhancement cavity.
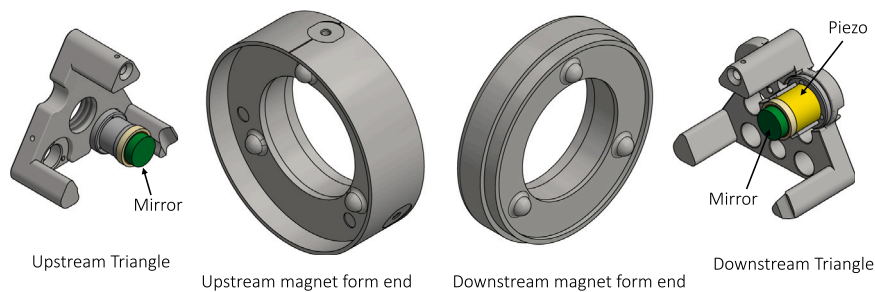

Fig. 21. From left to right: The upstream triangle, the upstream end of the magnet form, the downstream end of the magnet form, and the downstream triangle. Both triangles contain two slots for mounting a mirror assembly, but are shown with only one mirror assembly installed.

at 972 nm (1 kHz at 243 nm). The characteristic slow linear drift of the reference cavity is measured by the comb, and corrected by tuning the AOM frequency.

The short term linewidth of the laser is measured by beating the spectroscopy laser against an independent and identical 972 nm ECDL locked to an independent and identical ultra-stable reference cavity. The beat note generated between the two lasers has a spectrum composed of sub-Hz lines separated by 75 Hz within a 300 Hz (1.2 kHz at 243 nm) full-width half-maximum Gaussian envelope. The source of the linewidth broadening has been found to be acoustic noise within the laser laboratory, and subsequent work has reduced this effect.

3.8.2. The 1S-2P laser system

The 1S-2P laser system produces pulsed 121.6 nm light used to drive the corresponding Lyman-α antihydrogen transition and to perform laser cooling of the anti-atoms. We summarise the system here, and more details have been previously described elsewhere [92]. The laser arrangement and aspects of the associated optical elements are shown schematically in Fig. 22. A Ti:Sapphire crystal amplifier (based upon a pulsed, frequency-doubled Nd:YAG laser at 532 nm with a 10–50 Hz repetition rate) is seeded using a CW 729.4 nm diode laser with a bandwidth below 1 MHz. The 729.4 nm pulses are used for second harmonic generation (SHG) at 364.7 nm using a coated BBO crystal.
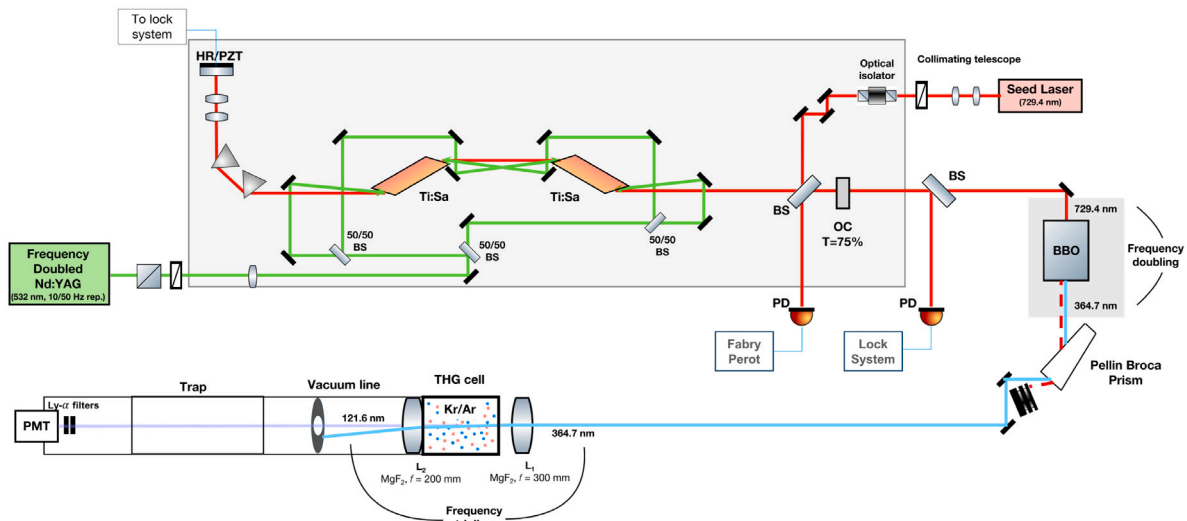
Fig. 22. Schematic of the laser arrangement and associated optics used by ALPHA to produce Lyman-α light for excitation of the $1S$-$2P$ transition in antihydrogen. The Ti:Sapphire crystals are pumped from both sides by the Nd:YAG laser (with the power distributed evenly between the four arms) and the amplified output exits via an output coupler (OC) to the BBO crystal. Note that the cavity contains a high reflector (HR) and two isosceles Brewster prisms, with the beam splitter (BS) having a transmission of 97%. The two MgF$_2$ lenses (L1 and L2 in the THG chamber) have focal lengths of 200 and 300 mm, respectively. Not shown in the figure are two irises between L2 and the solar-blind PMT (Hamamatsu R972) to remove unwanted 364.7 nm light from the beam.

This light is then separated from the fundamental using a pair of Pellin Broca prisms and is further directed into a gas cell for third harmonic generation (THG) of the desired 121.6 nm light. The 121.6 nm laser power is measured using solar blind photomultiplier tubes (PMTs) with appropriate filtering.

The Lyman-α laser pulses are generated using non-resonant THG in a gas cell containing a mixture of krypton and argon gases. Magnesium fluoride optical components are used to provide the beam intensities required to efficiently produce the vacuum ultra-violet radiation. Performance parameters of the PMT (i.e., response function, gain and quantum efficiency) are used to extract the temporal profile and pulse energy of the Lyman-α beam. The gas ratio and total pressure of the gas cell is experimentally determined to maximise the Lyman-α laser energy by adjusting the phase-matching condition for the THG process. The 121 nm and 365 nm pulses are separated from one another by injecting the 365 nm laser into the gas cell off-axis, and then blocking the 365 nm light with a set of irises.

Early performance of the SHG step resulted in pulse energies of around 18.0 mJ (with a standard deviation of about 1.4 mJ) for a Nd:YAG pulse energy of 310 mJ: pulse time widths are around 20 ns. A somewhat lower Nd:YAG energy of 250 mJ, combined with a novel off-resonant cavity locking condition, resulted in optimal overall performance for the Lyman-α power. The result was a 121.6 nm pulse of 11 ns time width with an energy of 6 nJ measured after the THG cell and 2 nJ inside the Atom Trap, with an overall linewidth below 100 MHz.

The pulsed light enters the Mixing and Atom Trap via a magnesium fluoride window and crosses a region near the centre at an angle of about 2° with respect to the trap axis. The antihydrogen $1S_d$-$2P_a$ transition was excited (which provides a closed cycle by avoiding de-excitation to an untrapped ground state) red-shifted by around 240 MHz to produce the required anti-atom cooling.

Further technical details can be found in [92].

3.9. Microwave systems and access

Microwaves are produced using an Agilent 8257D PSG analog signal generator and directed down one of two potential paths: a high power path with a Miteq AMF-4B 4 W amplifier for antihydrogen spectroscopy experiments, and a low-power path with no amplification for electron cyclotron resonance measurements of in-situ magnetic field strengths. These two paths are merged and enter the ultra-high vacuum region of the apparatus through a custom-built vacuum window, propagate down an internal waveguide, and finally enter the Penning trap electrodes and the antihydrogen trapping region. More details of the microwave injection system and its use have been described elsewhere [26].

3.10. The silicon vertex detector

The Silicon Vertex Detector (SVD) [93] is the primary diagnostic tool for antihydrogen physics studies in ALPHA-2. Antihydrogen atoms annihilate when they come into contact with matter, producing a variety of by-products. These by-products typically include 3–4 energetic charged pions, which are able to fully traverse the dense material surrounding the trap and pass through the SVD. These passing pions excite electron–hole pairs within the SVD's (reverse-biased) silicon strips, and the resulting signals are processed and recorded. The recorded data are subsequently analysed to reconstruct the time and location (vertex) of the original antihydrogen annihilation event.

3.10.1. SVD electronics and geometry

The detector is constructed from 72 hybrid modules arranged in a three-layered barrel shape, as shown in Fig. 23 [93,94]. Each hybrid module is equipped with two Double Sided Silicon-Strip Detectors (DSSD's), which contain 256×128 p-on-n strips with an active area of 58.1×112 mm. The two DSSDs are wire bonded together, effectively forming a 256×256 detector. Altogether, therefore, the SVD has a 4.7 megapixel resolution.

The barrel shaped detector structure has an active length of 448 mm and the modules are fitted in radii spanning from 89 to 132.5 mm. The layout covers a solid angle of 77% (9.67 sr) as seen from the centre of the Atom Trap (assuming track candidates must pass through active detector area in all three layers).

The SVD spatial resolutions for identifying a single hit are 66 µm and 253 µm in the ϕ- and (axial) z-directions, respectively. This spatial resolution was determined using a Monte Carlo simulation which included the detector geometry and the pion scattering in the materials between trap and the detector [93].

The data are collected through a chain of electronics, following the logical layout illustrated in Fig. 24. In addition to the two DSSD's
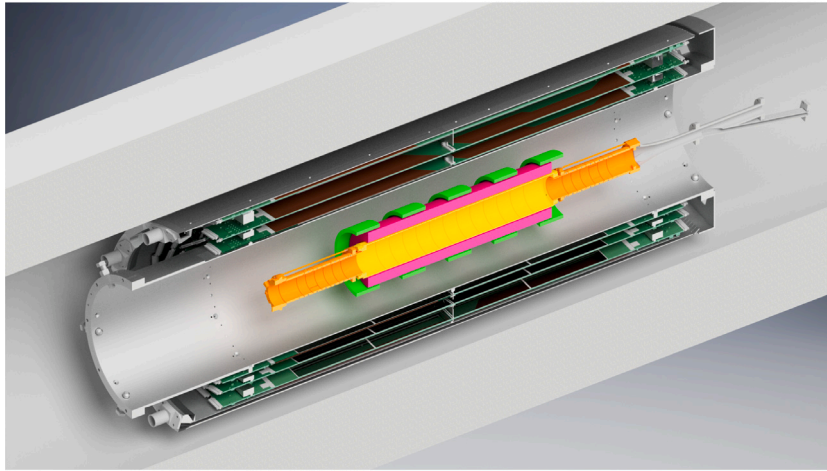
Fig. 23. Cut-through of the ALPHA Mixing and Atom Trap. The SVD (green) is located at atmospheric pressure between the outer beam pipe and the inner magnet bore. The hybrid modules are staggered in the azimuthal direction in order to improve the solid angle coverage. A ray-tracing simulation showed that the coverage was improved in the staggered case by around 6% when compared to the full solid angle. The radial distance of each layer from the centre is reduced by staggering, resulting in the increased coverage, despite the shadowing effects introduced.
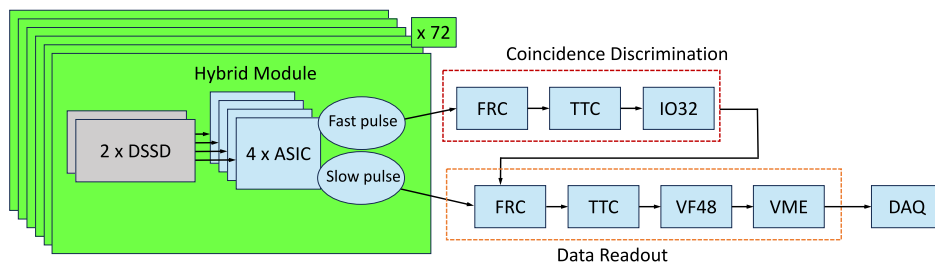

Fig. 24. Block diagram of the SVD readout system. Signals originate from particles depositing energy in the active area of the Silicon modules (DSSD). The signals are shaped by two independent integrated circuits on the same ASIC, which yield a fast and slow pulse. The former is compared to a fixed threshold, typically equivalent to 4800 electron–hole pairs, and the sum over the 128 channels is processed by an amplifier (FRC) and the timing module (TTC) for multiplicity trigger calculation. The final trigger decision is made by an FPGA (IO32) to determine whether the global multiplicity trigger condition is met. When this is the case, a readout trigger is sent to the FRC, prompting the sampling and multiplexing of the slow pulse data from the ASIC. While the analog readout has a fixed dead time of 40 μs (due to reading 128 strips serially with a 3.33 MHz clock), the limiting factor in the maximum event readout rate is due to the speed of the data transfer on the VME bus.

(which comprise the active detection area), each hybrid module contains four 128-channel VA1Ta (designed and manufactured by the integrated circuits company IDEAS in Olso, Norway) Application Specific Integrated Circuits (ASICs) which read the signal from the DSSD's. Each ASIC produces a fast digital pulse (trigger) and a slow (~1 μs) analog signal (readout) multiplexed over 128 channels (strips). The triggers and the multiplexed readouts are amplified by Front end Repeater Cards (FRCs). The triggers are passed to two Timing and Trigger Control units (TTCs) which analyse the multiplicity criteria for each layer and coordinate the analog readout. The FRCs, the TTCs and the IO32 boards are custom electronics designed and manufactured at TRIUMF in Vancouver (Canada). A VME FPGA-based board (IO32) performs the final decision to trigger the readout. When the readout is triggered, a hold signal is broadcast to all the ASICs via the FRC boards. TTCs then control the analog readout of the signals from the ASICs which are passed to eight 48-channel pulse shape digitisers VF48 [95]. The transfer of the digitised data is controlled by a VME single board computer (model GE Fanuc V7805) connected through Gigabit Ethernet to a local server for temporary storage and processing. The VME controller coordinates the data acquisition and initiates the readout of the detector data. To match the timing of the traps' operation with the SVD data, the Digital Sequencer (see Section 3.1.5) sends a trigger at the beginning and at the end of any given operation to a pair of VME multi-channel scalers SIS3820, manufactured by Struck Innovative Systeme GmbH. The scalers are read out on the same VME bus as the SVD data acquisition. The scalers are synchronised by using an external reference clock, typically achieving a timestamping

accuracy of 10^{-6} s. Additionally, the scalers are used to record the time of counts of the annihilation detectors (scintillators paddles), as described in Section 3.1.8. The detector's data acquisition system is integrated with the apparatus slow monitoring system and the trap controls in the MIDAS framework [96]. This system can read out the detector at more than 470 times per second.

Thus, the detector's performance in the time domain is limited by (a) a 1 μs resolution on single hit timing, (b) a minimum time between events of 40 μs, and (c) a maximum global readout rate of 470 Hz for the digitised data which contains 4.7 megapixels of information.

3.10.2. Cosmic ray rejection

Antihydrogen experiments typically involve counting anti-atom annihilations within specific time windows. This time window statistically includes some cosmic ray background that trigger the detector at an average rate of 9.8 events per second. Since the cosmic ray events are interleaved with signal, special attention is given to cosmic ray background rejection. The geometry of reconstructed tracks of a cosmic event is typically very different from that produced by an annihilation, as illustrated in Fig. 25, and can usually be readily distinguished (see also [97]). However, a small fraction of these events mimic the signature produced by annihilation due to scattering interactions within the inner apparatus. The original cosmic background rejection schemes are extensively described elsewhere [12,98]. Machine learning applied to ALPHA-2 detector data is continually developed [99] to improve cosmic ray rejection, and specific methods are described in the publications that employ them [21,22,26–29].
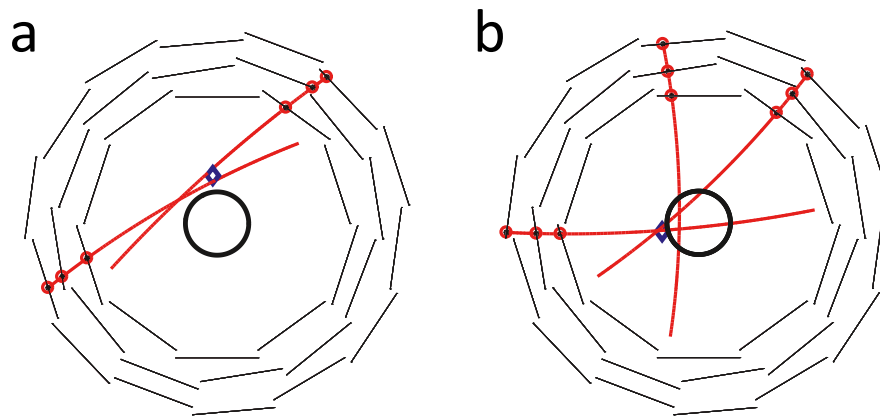
Fig. 25. The SVD reconstruction of (a) a typical cosmic ray event, and (b) a typical annihilation event. The red circles show the particle hit positions in the silicon modules, with the red lines the reconstructed tracks. The blue diamond indicates the inferred vertex position. The black inner ring marks the Atom Trap wall.

4. Concluding remarks

The ALPHA-2 apparatus has been described in detail. It has been used for pioneering studies of the physics of antihydrogen, including the first laser spectroscopic studies of its $1S$-$2S$ and $1S$-$2P$ transitions, exploration of the ground state hyperfine structure, and for laser cooling of the anti-atoms. Accumulation of samples of up to 10^3 antihydrogen atoms have been achieved, with lifetimes against loss of over 60 h. More recently the collaboration has worked to update the apparatus further, in particular to install a vertically oriented apparatus (ALPHA-g [31,33]) to perform improved measurements of antimatter gravity. The beamline modifications and magnet system associated with this new experiment have been reported elsewhere [83]. Given the strong performance record of ALPHA-2, and the recent physics successes (documented briefly in Section 1), we can look forward to much progress with the application of the capabilities of the ELENA facility to spectroscopic studies of antihydrogen [32].

CRediT authorship contribution statement

R. Akbari: Investigation. **B.X.R. Alves:** Investigation. **C.J. Baker:** Investigation, Writing – Original Draft. **M. Baquero-Ruiz:** Investigation. **W. Bertsche:** Investigation, Conceptualization, Writing – Original Draft. **E. Butler:** Investigation, Conceptualization. **C. Burrows:** Investigation. **A. Capra:** Investigation. **C.L. Cesar:** Investigation, Conceptualization. **M. Charlton:** Writing – review & editing, Investigation, Conceptualization. **R. Collister:** Investigation. **A. Cridland:** Investigation. **S. Eriksson:** Investigation, Conceptualization, Writing – Original Draft. **A. Evans:** Investigation, Conceptualization. **L.T. Evans:** Investigation. **N. Evetts:** Investigation. **J. Fajans:** Investigation, Conceptualization. **T. Friesen:** Investigation, Conceptualization. **M.C. Fujiwara:** Investigation, Conceptualization. **D.R. Gill:** Investigation. **P. Grandemange:** Investigation. **P. Granum:** Investigation. **A. Gutierrez:** Investigation. **J.S. Hangst:** Supervision, Resources, Project administration, Methodology, Investigation, Funding acquisition, Conceptualization. **M.E. Hayden:** Investigation, Conceptualization. **D. Hodgkinson:** Investigation. **C.A. Isaac:** Investigation. **A. Ishida:** Investigation. **M.A. Johnson:** Investigation. **J.M. Jones:** Investigation. **S.A. Jones:** Investigation, Conceptualization, Writing – Original Draft. **S. Jonsell:** Investigation. **A. Khramov:** Investigation. **L. Kurchaninov:** Investigation. **A. Little:** Investigation. **N. Madsen:** Investigation, Conceptualization, Writing – Original Draft. **D. Maxwell:** Investigation, Writing – Original Draft. **J.T.K. McKenna:** Investigation, Conceptualization, Writing – Original Draft. **S. Menary:** Investigation. **J.M. Michan:** Investigation. **T. Momose:** Investigation. **P.S. Mullan:** Investigation. **K. Olchanski:** Investigation. **A. Olin:** Investigation. **J. Peszka:** Investigation. **A. Povilus:** Investigation. **A. Powell:** Investigation. **P. Pusa:** Investigation, Writing – Original Draft. **C.Ø. Rasmussen:** Investigation, Conceptualization, Writing – Original Draft. **R.L. Sacramento:** Investigation. **M. Sameed:** Investigation, Writing – Original Draft. **E. Sarid:** Investigation, Writing – Original Draft. **D.M. Silveira:** Investigation. **C. So:** Investigation, Writing – Original Draft. **S. Stracka:** Investigation. **G. Stutter:** Investigation. **T.D. Tharp:** Writing – review & editing, Investigation, Writing – Original Draft. **R.I. Thompson:** Investigation. **C. Torkzaban:** Investigation. **D.P. van der Werf:** Investigation. **J.S. Wurtele:** Investigation.

Declaration of competing interest

The authors declare that they have no known competing financial interests or personal relationships that could have appeared to influence the work reported in this paper.

Acknowledgements

Data availability

Data will be made available on request.

References

[1] M. Amoretti, et al., ATHENA Collaboration, Nat. 419 (2002) 456.
[2] G. Gabrielse, et al., ATRAP Collaboration, Phys. Rev. Lett. 89 (2002) 213401.
[3] G. Gabrielse, et al., ATRAP Collaboration, Phys. Rev. Lett. 89 (2002) 233401.
[4] G. Gabrielse, et al., ATRAP Collaboration, Phys. Rev. Lett. 93 (2004) 073401.
[5] M. Amoretti, et al., ATHENA Collaboration, Phys. Lett. B 590 (2004) 133.
[6] M. Amoretti, et al., ATHENA Collaboration, Phys. Lett. B 578 (2004) 23.
[7] N. Madsen, et al., ATHENA Collaboration, Phys. Rev. Lett. 94 (2005) 033403.
[8] M.C. Fujiwara, et al., ATHENA Collaboration, Phys. Rev. Lett. 92 (2004) 065005.
[9] R. Funakoshi, et al., ATHENA Collaboration, Phys. Rev. A 76 (2007) 012713.
[10] M.C. Fujiwara, et al., ATHENA Collaboration, Phys. Rev. Lett. 101 (2008) 053401.
[11] M. Amoretti, et al., ATHENA Collaboration, Nucl. Inst. Meth. A 518 (2004) 679.
[12] C. Amole, et al., ALPHA Collaboration, Nucl. Inst. Meth. A 735 (2014) 319.
[13] G.B. Andresen, et al., ALPHA Collaboration, Nat. 468 (2010) 673.

[14] G.B. Andresen, et al., ALPHA Collaboration, Phys. Letts B 695 (2011) 95.

[15] G.B. Andresen, et al., ALPHA Collaboration, Nat. Phys. 7 (2011) 55.

[16] M. Ahmadi, et al., ALPHA Collaboration, Nat. Commun. 8 (2017) 681.

[17] M. Ahmadi, et al., ALPHA Collaboration, Nat. 561 (2018) 211.

[18] G. Gabrielse, et al., ATRAP Collaboration, Phys. Rev. Lett. 108 (2012) 113002.

[19] C. Amole, et al., ALPHA Collaboration, Nat. 483 (2012) 439.

[20] C. Amole, et al., ALPHA Collaboration, Nat. Commun. 4 (2013) 1785.

[21] C. Amole, et al., ALPHA Collaboration, Nat. Commun. 5 (2014) 3955.

[22] M. Ahmadi, et al., ALPHA Collaboration, Nat. 529 (2016) 373.

[23] M. Charlton, in: L. Dorikens Vanpraet, M. Dorikens, D. Segers (Eds.), Positron Annihilation, World Scientific, Singapore, 1988, p. 181.

[24] G. Gabrielse, S.L. Rolston, L. Haarsma, W. Kells, Hyperfine Interact. 44 (1988) 287.

[25] Ch.G. Parthey, A. Matveev, J. Alnis, B. Bernhardt, A. Beyer, R. Holzwarth, A. Maistrou, R. Pohl, K. Predehl, Th. Udem, T. Wilken, N. Kolachevsky, M. Abgrall, D. Rovera, Ch. Salomon, P. Laurent, T.W. Hänsch, Phys. Rev. Lett. 107 (2011) 203001.

[26] M. Ahmadi, et al., ALPHA Collaboration, Nat. 548 (2017) 66.

[27] M. Ahmadi, et al., ALPHA Collaboration, Nat. 541 (2017) 506.

[28] M. Ahmadi, et al., ALPHA Collaboration, Nat. 557 (2018) 71.

[29] C.J. Baker, et al., ALPHA Collaboration, Nat. 592 (2021) 35.

[30] C.J. Baker, et al., ALPHA Collaboration, Precision spectroscopy of the hyperfine components of the 1s-2s transition in antihydrogen, Nat. Phys. (2025) http://dx.doi.org/10.1038/s41567-024-02712-9, in press.

[31] W.A. Bertsche, Phil. Trans. R. Soc. A 376 (2018) 20170265.

[32] Antiproton physics in the ELENA era, A Theo Murphy meeting issue organized and edited by Niels Madsen, Phil. Trans. R. Soc. A 376 (2018).

[33] E.K. Anderson, et al., ALPHA Collaboration, Nat. 621 (2023) 716.

[34] C. Amsler, et al., AEgIS Collaboration, Nat. Commun. 4 (2021) 19.

[35] P. Adrich, et al., GBAR Collaboration, Eur. Phys. J. C 83 (2023) 1004.

[36] N. Kuroda, et al., ASACUSA Collaboration, Nat. Commun. 5 (2014) 3089.

[37] L. Nowak, et al., ASACUSA Collaboration, Phys. Lett. B 858 (2024) 139012.

[38] A. Soter, et al., ASACUSA Collaboration, Nat. 603 (2022) 411.

[39] G. Borchert, et al., BASE Collaboration, Nat. 601 (2022) 53.

[40] C. Smorra, et al., BASE Collaboration, Nat. 550 (2017) 371.

[41] G. Schneider, et al., BASE Collaboration, Sci. 358 (2017) 1081.

[42] T. Aumann, et al., PUMA Collaboration, Eur. Phys. J. A 58 (2022) 88.

[43] S. Maury, Hyperfine Interact. 109 (1997) 43.

[44] W. Oelert, T. Eriksson, P. Belochitskii, G. Tranquille, Hyperfine Interact. 213 (2012) 227.

[45] W. Bartmann, et al., on behalf of the ELENA and AD teams, Phil. Trans R. Soc. A 376 (2018) 20170266.

[46] G.B. Andresen, et al., ALPHA Collaboration, Phys. Rev. Lett. 100 (2008) 203401.

[47] G.B. Andresen, et al., ALPHA Collaboration, Phys. Rev. Lett. 105 (2010) 013003.

[48] S. Maury, et al., Hyperfine Interact. 229 (2014) 105.

[49] L.V. Jørgensen, et al., ATHENA Collaboration, Phys. Rev. Lett. 95 (2005) 025002.

[50] J.R. Danielson, D.H.E. Dubin, R.G. Greaves, C.M. Surko, Rev. Mod. Phys. 87 (2015) 247.

[51] C.M. Surko, R.G. Greaves, M. Charlton, Hyperfine Interact. 109 (1997) 181.

[52] Y. Enomoto, et al., Phys. Rev. Lett. 105 (2010) 243401.

[53] S. Aghion, et al., AEgIS Collaboration, Nucl. Inst. Meth. B 362 (2015) 86.

[54] S. Niang, et al., GBAR Collaboration, Acta Phys. Pol. A 137 (2020) 164.

[55] D.W. Fitzakerley, et al., ATRAP Collaboration, J. Phys. B: At. Mol. Opt. Phys. 49 (2016) 064001.

[56] P. Blumer, et al., GBAR Collaboration, Nucl. Inst. Meth. A 1040 (2022) 167263.

[57] R.G. Greaves, C.M. Surko, Phys. Rev. Lett. 85 (2000) 1883.

[58] R.G. Greaves, C.M. Surko, Phys. Plasmas 8 (2000) 1879.

[59] J.R. Danielson, C.M. Surko, Phys. Rev. Lett. 94 (2005) 035001.

[60] J.R. Danielson, C.M. Surko, T.M. O'Neil, Phys. Rev. Lett. 99 (2007) 135005.

[61] M. Ahmadi, et al., ALPHA Collaboration, Phys. Rev. Lett. 120 (2018) 025001.

[62] J. Fajans, K. Burke, W. Bertsche, S.F. Chapman, D.P. van der Werf, Phys. Rev. Lett. 95 (2005) 155001.

[63] X. Fei, Trapping Low Energy Antiprotons in an Ion Trap (Ph.D. thesis), Harvard University, 1990.

[64] Chr. Day, A. Antipenkov, M. Dremel, H. Haas, V. Hauer, A. Mack, D.K. Murdoch, M. Wyke, Vacuum 81 (2007) 738.

[65] W. Thompson, S. Hanrahan, J. Vac. Sci. Technol. 14 (1977) 643.

[66] A. Capra, et al., ALPHA collaboration, Hyperfine Interact. 240 (2019) 9.

[67] C. Smorra, et al., BASE Collaboration, Int. J. Mass Spec. 389 (2015).

[68] G.B. Andresen, et al., ALPHA Collaboration, Rev. Sci. Instrum. 80 (2009) 123701.

[69] Data from ALPHA datalog 72196 (electrons) and datalog 72210 (antiprotons). Datalog 72211 was used to determine the total number of antiprotons.

[70] T.J. Murphy, C.M. Surko, Phys. Rev. A 46 (1992) 5696.

[71] A.P. Mills Jr., E.M. Gullikson, Appl. Phys. Lett. 49 (1986) 1121.

[72] R. Khatri, M. Charlton, P. Sferlazzo, K.G. Lynn, A.P. Mills Jr., L.O. Roellig, Appl. Phys. Lett. 57 (1990) 2374.

[73] C.J. Baker, C.A. Isaac, D. Edwards, H.T. Evans, R. Clayton, D.P. van der Werf, M. Charlton, J. Phys. B: At. Mol. Opt. Phys. 53 (2020) 185201.

[74] J.P. Marler, C.M. Surko, Phys. Rev. A 72 (2005) 062713.

[75] X.-P. Huang, F. Anderegg, E.M. Hollman, C.F. Driscoll, Phys. Rev. Lett. 78 (1997) 875.

[76] E.M. Hollman, F. Anderegg, C.F. Driscoll, Phys. Plasmas 7 (2000) 2776.

[77] D.P. van der Werf, C.A. Isaac, C.J. Baker, T. Mortensen, S.J. Kerrigan, M. Charlton, New J. Phys. 14 (2012) 075022.

[78] C. Amole, et al., ALPHA Collaboration, New J. Phys. 16 (2014) 013037.

[79] G.B. Andresen, et al., ALPHA Collaboration, Phys. Rev. Lett. 106 (2011) 025002.

[80] D.L. Eggleston, C.F. Driscoll, B.R. Beck, A.W. Hyatt, J.H. Malmberg, Phys. Fluids B 4 (1992) 3432.

[81] S. Jonsell, M. Charlton, J. Phys. B: At. Mol. Opt. Phys. 54 (2021) 025001.

[82] C. Amole, et al., ALPHA Collaboration, Phys. Plasmas 20 (2013) 043510.

[83] C.J. Baker, et al., ALPHA Collaboration, Phys. Rev. Accel. Beams (2023) 26040101.

[84] Cobham Technical Services, Vector Fields Simulation Software, Kidlington, UK -http://www.cobham.com/about-cobham/communications-and-connectivity/about-us/antenna-systems/specialist-technical-services-and-software/products-and-services/design-simulation-software/applications.

[85] Sumera Yamin, Khalid Mansoor Hassan, CERN TE/MSC/MNC internal note 2012-22, EDMS 1235913, Design of compact solenoids for the ALPHA experiment.

[86] Attilio Milanese, Normal conducting solenoid (type 2) for the ALPHA experiment, CERN-ATS-Note-2012-100-TECH, EDMS 1257534.

[87] N. Evetts, P. Dosanjh, V. Zvyagintstev, W.N. Hardy, Rev. Sci. Instrum. 86 (2015) 126101.

[88] C.Ø. Rasmussen, N. Madsen, F. Robicheaux, J. Phys. B: At. Mol. Opt. Phys. 50 (2017) 184002; J. Phys. B: At. Mol. Opt. Phys. 51 (2018) 099501, and corrigendum.

[89] S.A. Jones, Observation of the 1S-2S Transition in Trapped Antihydrogen (Ph.D. thesis), Swansea University, 2017.

[90] A.N. Oliveira, L.S. Moreira, R.L. Sacramento, L. Kosulic, V.B. Brasil, W. Wolff, C.L. Cesar, Rev. Sci. Instrum. 88 (2017) 063104.

[91] R. Drever, J.L. Hall, F.V. Kowalski, J. Hough, G.M. Ford, A.J. Munley, H. Ward, Appl. Phys. B: Lasers Opt. 31 (1983) 97.

[92] J.M. Michan, G. Polovy, K.W. Madison, M.C. Fujiwara, T. Mamose, Hyperfine Interact. 235 (2015) 29.

[93] C. Amole, et al., ALPHA Collaboration, Nucl. Inst. Meth. A 732 (2013) 134.

[94] G.B. Andresen, et al., ALPHA Collaboration, J. Instrum. 7 (2012) C01051.

[95] J.P. Martin, P.A. Amaudruz, IEEE Trans. Nucl. Sci. 53 (2006) 715.

[96] S. Ritt, P. Amaudruz, K. Olchanski, Proc. IEEE 10th Real Time Conf, 1997, p. 309.

[97] A. Capra, Testing CPT and Antigravity with Trapped Antihydrogen at ALPHA (Ph.D. thesis), York University, Toronto.

[98] G.B. Andresen, et al., ALPHA Collaboration, Nucl. Inst. Meth. A 684 (2012) 73.

[99] A. Capra, et al., ALPHA Collaboration, J. Phys: Conf. Ser. 1085 (2018) 042007.